Chapter 4

Results and Discussion

4.1 Differential Cross Sections for Monatomics

To validate the new SSRDM normalisation techniques, the DCSs for a series of stable targets were measured. The pyrolysis nozzle was thus removed from the system for these measurements so that all the targets were initially at room temperature. The DCSs of the chosen targets were all previously established in the literature from effusive beam measurements employing the Relative Flow Method [55]. The chosen targets are also generally well described by the theoretical calculations available in the literature. The first target considered was the monatomic species Ar. A series of molecular targets were then studied in order of increasing number of fundamental vibrational modes, so as to progressively increase the complexity of the normalisation procedure.

In forming supersonic jets, a practice often used in previously reported experiments is to dilute the target molecule with a carrier gas, typically a lighter species such as He or Ar. By diluting, or "seeding", the target gas with a carrier gas, the heavier species can reach a higher velocity than would have been achieved in a pure expansion of the target under equivalent stagnation conditions. As a result, the target molecule is cooled to a lower temperature than that achieved in a pure expansion.

For the experiments reported in this thesis, carrier gases were not used to form the molecular beams. The reason for avoiding carrier gases is that elastic electron scattering from the carrier gas molecules cannot be distinguished from elastic scattering by the target species. The contribution of the carrier species to the total elastic scattering signal would then have to be subtracted, based on the DCS of the carrier. Subtracting this contribution from the carrier would increase both the statistical and absolute uncertainties in the final measured DCS. Therefore, to ensure statistically meaningful experiments could be acquired within reasonable data acquisition times, the use of carrier gases was avoided.

4.1.1 Ar

The first test case for SSRDM normalisation was Ar, which contains no vibrational modes. In the absence of any internal structure the adiabatic constant is, without any ambiguity, evaluated as $\gamma = 5/3$ and the speed ratio is accurately determined by equation (3.2.17). Another advantage of monatomic targets is that the DCS can be normalised using both the p-SSRDM or t-SSRDM approaches, thus providing a cross-check in relation to the self consistency of the two approaches.

Absolute elastic DCSs, between 20-50 eV incident energy, for electron scattering from Ar were measured using He as a reference gas (Figures 4.1.1 and 4.1.2). These DCSs were normalised using both the p-SSRDM and t-SSRDM approaches. To ensure free molecular flow at the skimmer, Ar was introduced into the expansion chamber through the nozzle at a stagnation pressure of 130 mbar, with He subsequently introduced at a stagnation pressure of 460 mbar, in order to match the speed ratios (S_∞=19.4). Data was accumulated for one hour, for both the Ar and He measurements.

The pressure in the collision chamber when gas was admitted was approximately double the baseline pressure (1×10^{-7} Torr), for both gases. For the p-SSRDM normalisation, the relevant 150 eV ionisation cross sections were taken as

Q^{ion}=2.68 Å^2 [59] for Ar and Q^{ion}=0.33 Å^2 for He [60].

To prevent clusters forming in these measurements the stagnation pressures for the He and Ar beams were set such that the dimer formation parameter, D^*, was less than 0.1. At this level, the total concentration of dimers in the target beam is less than 1% [42]. The dimer formation parameter is given as:

$$D^* = \frac{P_0 \sigma^3}{\epsilon} \left(\frac{d}{\sigma} \right)^{0.4} \left(\frac{\epsilon}{T_0 k_{\mathrm{B}}} \right)^{2.4} \tag{4.1.1}$$

where σ and ϵ are the standard parameters of a Lennard-Jones potential, i.e. the finite distance of zero intermolecular force and the depth of the intermolecular well, respectively [42]. Under the present stagnation conditions, the dimer formation parameters for Ar and He were evaluated as 3.7×10^{-3} and 2.0×10^{-4}, respectively.

Both the p-SSRDM and t-SSRDM normalisation methods were applied to data from the same experimental run, with the DCSs determined at several incident energies being given in Table 4.1. The total uncertainty in the p-SSRDM normalised data is approximately 15%, here determined as the quadrature sum of statistical uncertainties ($<$5%), normalisation uncertainties (8%) and the uncertainty on the He elastic DCS (7%). For the t-SSRDM normalisation, the total uncertainty is about 10%, with the normalisation uncertainties now about 4%, and all the other uncertainties remaining the same as those listed.

The measured Ar elastic DCS, using both the p-SSRDM and t-SSRDM normalisations, are compared to two previous results from effusive beam measurements [61, 62] and from an R-Matrix calculation [63]. Both normalisation techniques give results which are consistent with the previous measurements, to within the limits of the combined uncertainties, at most angles and energies. These results are in similarly good accord with those from the R-Matrix calculation.

Table 4.1: Absolute elastic DCSs for electron scattering from Ar. The cross sections (σ) and their respective absolute uncertainties ($\Delta\sigma$) are in units of $\text{Å}^2\ sr^{-1}$. Cross sections were determined by both the p-SSRDM and t-SSRDM approaches.

| Angle | p-SSRDM | | | | | | | | t-SSRDM | | | |
| | 20eV | | 30eV | | 40eV | | 50eV | | 30eV | | 50eV | |
	σ	$\Delta\sigma$	σ	$\Delta\sigma$	σ	$\Delta\sigma$	σ	$\Delta\sigma$	σ	$\Delta\sigma$	σ	$\Delta\sigma$
20°	8.500	3.000	8.600	1.200	5.090	0.990	4.500	0.920	6.850	0.690	3.630	0.360
40°	5.600	1.400	2.660	0.340	1.690	0.230	1.250	0.170	2.130	0.210	1.000	0.100
60°	0.710	0.180	0.220	0.027	0.094	0.013	0.039	0.006	0.172	0.017	0.031	0.003
75°	0.214	0.050	0.076	0.010	0.109	0.014	0.118	0.016	0.061	0.006	0.094	0.009
90°	0.650	0.160	0.430	0.054	0.420	0.057	0.378	0.051	0.339	0.034	0.302	0.030
105°	0.680	0.170	0.560	0.075	0.510	0.070	0.384	0.053	0.450	0.045	0.307	0.031
120°	0.450	0.110	0.327	0.044	0.270	0.037	0.217	0.031	0.261	0.026	0.173	0.017
135°	0.730	0.190	0.131	0.022	0.074	0.011	0.036	0.007	0.105	0.011	0.029	0.003
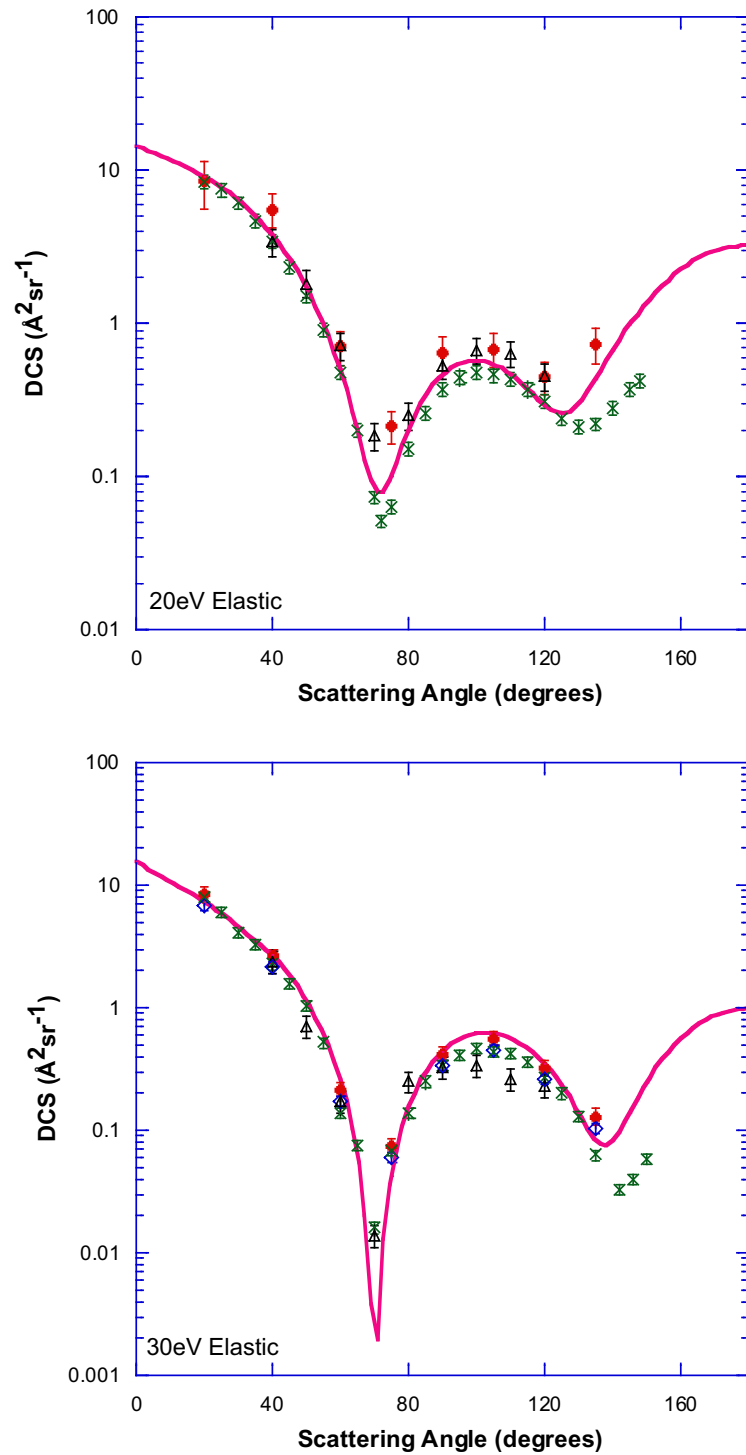
Figure 4.1.1: Absolute elastic DCS ($\text{Å}^2 sr^{-1}$) for electron scattering from Ar at incident energies of 20 and 30 eV. Present results obtained by both the p-SSRDM ($\bullet$) and t-SSRDM ($\diamond$) normalisations are shown. The results of two effusive beam measurements, [61] ($\times$) and [62] ($\triangle$), as well as an R-Matrix calculation [63] (solid Curve) are also shown.
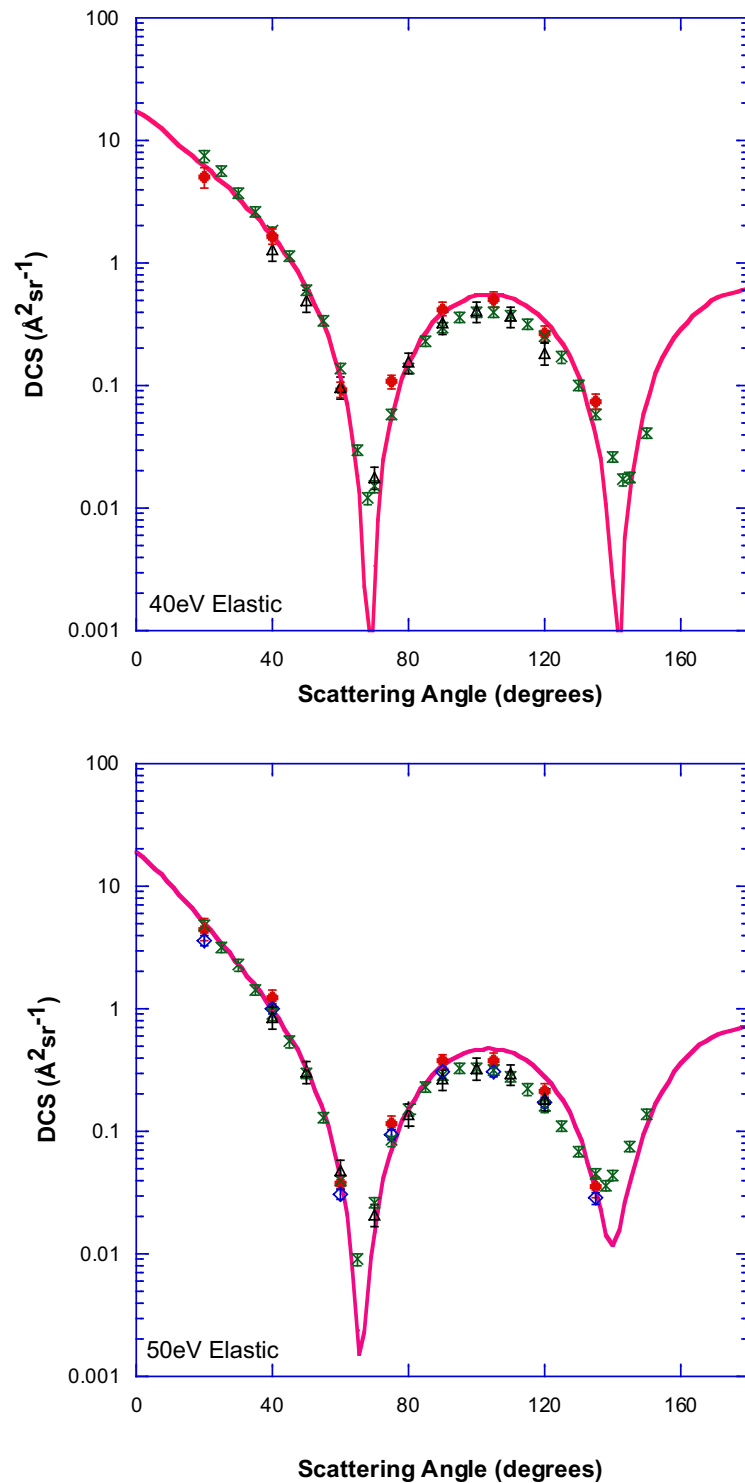
Figure 4.1.2: Absolute elastic DCS ($\text{Å}^2 sr^{-1}$) for electron scattering from Ar at incident energies of 40 and 50 eV. Present results obtained by both the p-SSRDM ($\bullet$) and t-SSRDM ($\diamond$) normalisations are shown. The results of two effusive beam measurements, [61] ($\times$) and [62] ($\triangle$), as well as an R-Matrix calculation [63] (solid curve) are also shown.

The previous comments notwithstanding, the normalisation of the Ar DCS by the p-SSRDM is consistently about 20% higher than that from the t-SSRDM. This result is, however, within the combined normalisation uncertainties ($\sim$25%). Hence, the two normalisation methods are concluded to be consistent with one another and in general the SSRDM approach is concluded to be able to accurately normalise the DCS for a structurally simple target.

4.2 Differential Cross Sections for Polyatomics

Having established the SSRDM approach for monatomic targets, the DCSs of several polyatomic targets were then measured. In principle, the DCSs for molecules are more challenging to accurately normalise by the SSRDM approach, compared to DCSs for atoms. This follows as for molecules, the speed ratios are not determined by an accurate calculation (equation (3.2.17)), but instead by an approximation (equation (3.2.10)) based on the stagnation pressure. Further, the adiabatic constant now has to include any fundamental rotational and vibrational modes which are significantly occupied at the stagnation temperature. For this thesis, 150 meV was chosen as the upper vibrational energy limit for a mode to be included in the the number of vibrational degrees of freedom, however, this was a subjective choice. Thus, for a polyatomic expansion, the parameters γ and S_∞ cannot be determined with the same degree of confidence as those for a monatomic expansion.

The rotational/vibrational relaxations in a molecule also increase the thermal velocity of the molecules during the expansion, due energy released during the internal relaxation. Therefore polyatomic expansions do not reach free molecular flow as close to the nozzle as was the case for monatomic expansions, under equivalent stagnation conditions, due to the increased thermal motion. The stagnation pressures employed for the polyatomic experiments were therefore all lower than that for the monatomic experiment to ensure that a quitting surface was formed prior to the skimmer. This presented three distinct disadvantages relative to the monatomic experiment. The first was that the pressure rise in the

collision chamber was not as high as for Ar, thus increasing the measurement uncertainties. The second was that the terminal speed ratios of the polyatomic expansions were all significantly lower than in the Ar experiment. As a result of the decreased speed ratio, ie. more thermal motion relative to the translational motion, the gas beam was less collimated at the interaction region. Finally, the electron scattering signal from the polyatomic beams was weaker than the monatomic measurement, as a result of the less dense gas beams. Therefore, the experiments had to be run for longer in order to achieve the same level of statistical precision. A final issue with molecules is that normalisation can only be achieved using the p-SSRDM approach, which is the less precise of the two methods.

In order to test SSRDM for polyatomics the DCSs of three molecules, with an increasing number of vibrational modes, were measured. The degree of complexity for achieving an accurate normalisation increases as the structural complexity of the molecule increases. Therefore, by successively increasing the number of fundamental rotational and vibrational modes available to the targets, the limits of SSRDM's applicability were tested. Also, within this paradigm, the targets chosen additionally represent typical feedstock gases used in industrial plasma reactors.

4.2.1 CF_4

The first molecule tested was CF_4. Tetrafluoromethane has only one rotational mode, due to its spherical symmetry, and four fundamental vibrational modes. All of these vibrational modes, bar the v_3 degenerate asymmetric stretch mode (159 meV) [26], are lower than the 150 meV exclusion threshold and are therefore included in evaluating the adiabatic constant. The adiabatic constant for CF_4 was hence evaluated as $\gamma=9/7$. There is little uncertainty in this value, since even including the v_3 vibrational mode only slightly decreases γ (to 10/8).

Absolute elastic DCSs for CF_4 were measured at incident energies between 15-50 eV (Figures 4.2.1 and 4.2.2), using the p-SSRDM normalisation with He employed as the reference species. In this work gas was introduced to the vacuum chamber at stagnation pressures of 120 mbar (S_∞=7.9) for CF_4 and 83 mbar for He. Data was accumulated over four hours for each of the CF_4 and He beams at each incident energy.

With a base pressure of 1.4×10^{-7} Torr, the pressure in the collision chamber when the gas was admitted was 6.0×10^{-7} Torr for CF_4 and 1.9×10^{-7} Torr for He. The ionisation cross section for CF_4 was taken as $Q_{CF_4}^{ion}$=5.71 Å^2 [29] for the p-SSRDM normalisation. The CF_4 dimer formation parameter was evaluated as $D_{CF_4}^*$=2.1$\times10^{-2}$ so that the cluster concentration was considered negligible.

The total uncertainty in the DCS measurements is approximately in the range 25–30%, determined as the quadrature sum of statistical uncertainties ($<$5%), normalisation uncertainties (20%) and the uncertainty of the He elastic DCS (7%). The $\approx$10% increase in the final DCS uncertainty, compared with Ar (15%), is due to the propogation of the 10% uncertainty in S_∞ which results from using equation (3.2.10). Thus, the uncertainty in the normalisation constant is higher in the case of CF_4 (20%), compared to Ar (8%).

The results of these DCS measurements, and their respective uncertainties, are given in Table 4.2 and plotted in Figures 4.2.1 and 4.2.2. The elastic DCSs for CF_4 are compared to two results from previous effusive beam measurements [64, 65], and also from two Schwinger Multichannel calculations (SMC) [66, 67]. The differences between the SSRDM normalised data and any of the previous results is generally less than the the experimental uncertainties in the present data. Indeed, the level of agreement between all of the data sets is generally very good. Thus, p-SSRDM was also considered to having been validated for a structurally simple molecule. However, the p-SSRDM does lose some precision when normalising for the DCS of a molecule, due to the weaker characterisation of the expansion parameters.
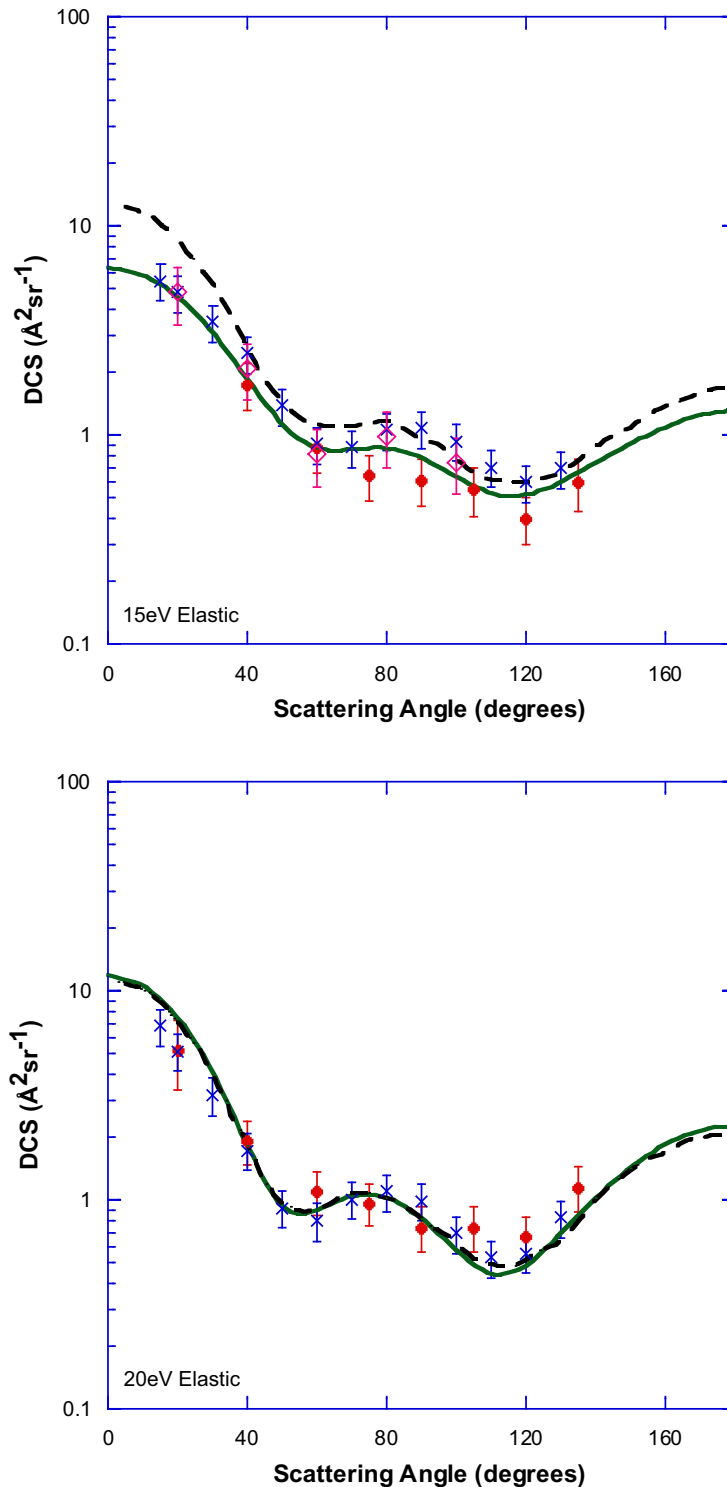
Figure 4.2.1: Absolute elastic DCS ($\mathring{A}^2 sr^{-1}$) for electron scattering from CF_4 at incident energies of 15 and 20 eV. Present results obtained by the p-SSRDM (•) normalisation are shown. The results of two effusive beam measurements, [64] (×) and [65] (◇), plus the two SMC calculations, [66] (solid curve) and [67] (dashed curve), are also shown.

Figure 4.2.2: Absolute elastic DCS ($\mathring{A}^2 sr^{-1}$) for electron scattering from CF_4 at incident energies of 30 and 50 eV. Present results obtained by the p-SSRDM ($\bullet$) normalisation are shown. The results of two effusive beam measurements, [64] ($\times$) and [65] ($\diamond$), plus the two SMC calculations, [66] (solid curve) and [67] (dashed curve), are also shown.
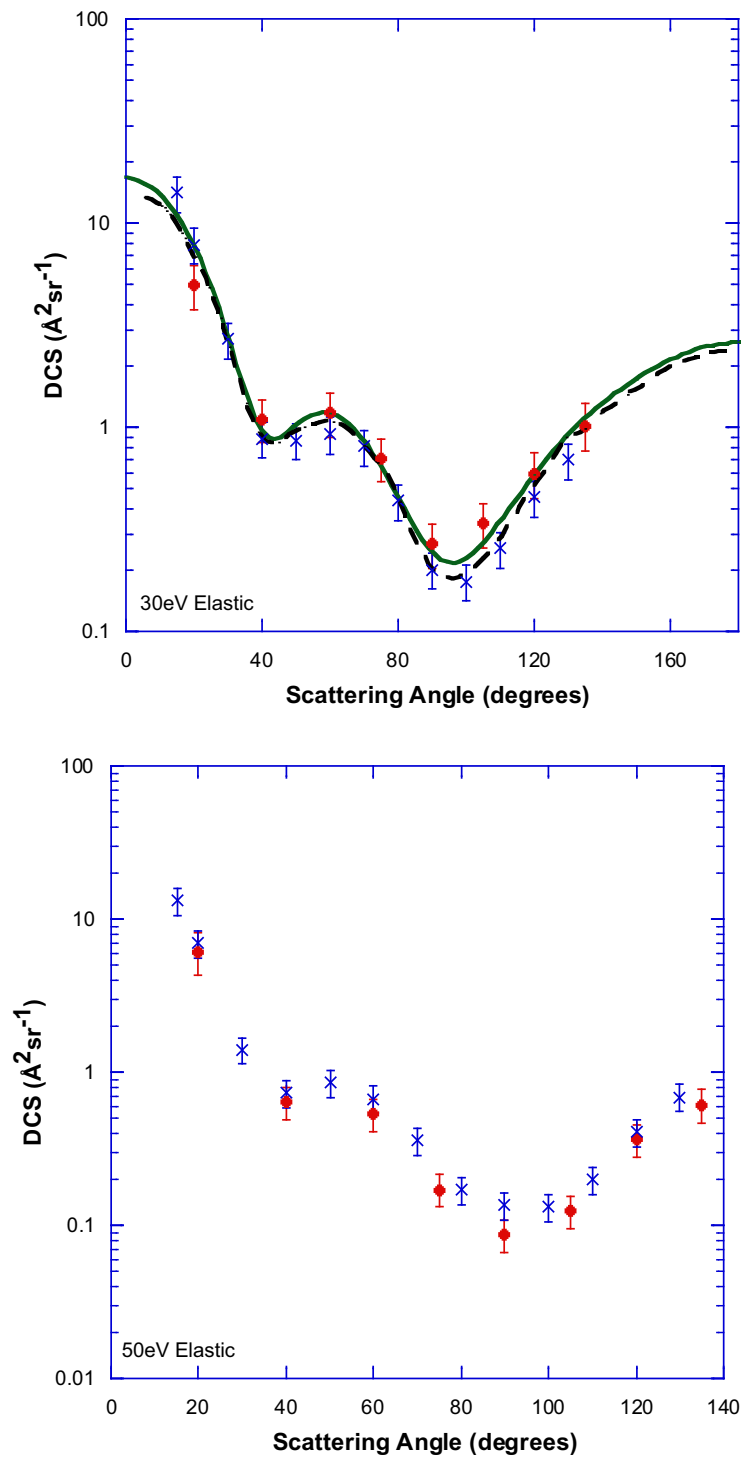
Table 4.2: Absolute elastic DCS for electron scattering from CF_4 at various energies as determined by p-SSRDM normalisation. The cross sections (σ) and their respective absolute uncertainties ($\Delta\sigma$) are in units of Å^2 sr^{-1}.

Angle	15eV		17.5eV		20eV		30eV		40eV		50eV	
	σ	$\Delta\sigma$	σ	$\Delta\sigma$	σ	$\Delta\sigma$	σ	$\Delta\sigma$	σ	$\Delta\sigma$	σ	$\Delta\sigma$
20°					5.100	1.500	5.000	1.200	9.000	2.300	6.200	1.900
40°	1.750	0.270	1.420	0.370	1.920	0.460	1.100	0.260	0.800	0.190	0.640	0.150
60°	0.870	0.210	0.990	0.240	1.100	0.026	1.180	0.280	0.900	0.210	0.540	0.130
75°	0.640	0.160	0.780	0.190	0.970	0.220	0.710	0.170	0.338	0.080	0.173	0.041
90°	0.610	0.170	0.670	0.160	0.740	0.180	0.269	0.064	0.119	0.028	0.087	0.021
105°	0.550	0.140	0.880	0.220	0.740	0.160	0.340	0.086	0.189	0.047	0.126	0.030
120°	0.400	0.100	0.760	0.190	0.670	0.160	0.600	0.150	0.430	0.110	0.367	0.087
135°	0.600	0.170	1.950	0.900	1.150	0.280	1.030	0.270	1.020	0.250	0.620	0.150

4.2.2 CF$_3$Br

The next molecule studied was CF$_3$Br, which has two additional vibrational modes plus one additional rotational mode than CF$_4$. Further, all six fundamental vibrational modes now fall below 150 eV [26] and are thus included in the adiabatic constant, to give γ=13/11. Note though that because the v$_4$ degenerate CF$_3$ stretch mode is at 150 meV, exactly on the exclusion threshold, including this mode is something of a point of ambiguity. As a result of the increased number of vibrational modes, the stagnation pressure employed for CF$_3$Br (35 mbar) was significantly lower than that for CF$_4$ (120 mbar) to ensure free flow at the skimmer. The terminal speed ratio of CF$_3$Br (S_∞=6.9) was therefore lower than for CF$_4$ (S_∞=8.8), with the He stagnation pressure required to match the speed ratio was also lower than that used in the CF$_4$ experiment. Thus, although CF$_4$ and CF$_3$Br are structurally similar molecules, in a supersonic expansion their dynamics are significantly different and they are treated differently by the SSRDM. This molecule therefore, in addition to the CF$_4$ data, provided a further stringent test of the SSRDM description of the expansion dynamics.

Absolute elastic DCSs for electron scattering from CF$_3$Br were measured at various energies between 15-50 eV (Figures 4.2.3 and 4.2.4), using the p-SSRDM normalisation with He employed as the reference species. Here, gas was admitted into the vacuum chamber at stagnation pressures of 35 mbar for CF$_3$Br (S_∞=6.9) and 40 mbar for He. Data was accumulated over four hours each for the CF$_3$Br and He beams, at each energy.

From a base pressure of 1.3×10^{-7} Torr, the pressure in the collision chamber once gas was introduced rose to 2.8×10^{-7} Torr for CF$_3$Br and 1.6×10^{-7} Torr for He. The CF$_3$Br ionisation cross section for the p-SSRDM normalisation was taken from a Deutsch-Märk (DM) formalism calculation as Q^{ion}=7.1 Å^2 [68]. The dimer formation parameter was not evaluated for CF$_3$Br, because accurate Lennard-Jones parameters for this molecule are unknown. However, given the

very low stagnation pressure, significant cluster concentration within the beam is unlikely.

The total uncertainty in the DCS measurements is in the range of 30-35%, determined as the quadrature sum of the statistical uncertainties ($<5\%$), normalisation uncertainties (25%) and the uncertainty of the He elastic DCS (7%). This normalisation uncertainty (25%) is higher than the corresponding uncertainty for both the CF_4 (20%) or Ar (8%) cases. In this instance the normalisation uncertainty is larger than for CF_4 primarily due to the low pressure rise in the collision chamber during the He measurement. With a pressure rise of only 23% for He, the uncertainty in the change in collision chamber pressure was calculated as 13%, compared to 8% for CF_4.

The results of these experiments are given in Table 4.3 and plotted in Figures 4.2.3 and 4.2.4. The present elastic DCSs for electron scattering from CF_3Br are compared to results from a previous effusive beam measurement [69], plus results from two theoretical calculations: an SMC including psuedo-potentials method (SMCPP) [70]; and a continuum multiple scaling method (CMS). The present results generally lie within the uncertainty limits of all three data sets. Note that the SMCPP exceeds the previous effusive beam measurement by significantly more then their experimental uncertainties at scattering angles $>40°$ in the 30 eV plot. However, the p-SSRDM normalised data is sufficiently higher than the effusive beam results, in this angular region, to bring the SMCPP results to within the present experimental uncertainties. Unfortunately, however, as the present uncertainty limits are large enough to also include the effusive beam results, the current data cannot be concluded to prefer either result.

4.2.3 C_2F_4

The final test case used to validate the SSRDM was C_2F_4, which is the most structurally complex molecule considered is the present study. This molecule has three fundamental rotational modes, plus twelve fundamental vibrational modes.

Table 4.3: Absolute elastic DCS for electron scattering from CF_3Br at various energies determined by the p-SSRDM normalisation. The cross sections (σ) and their respective absolute uncertainties ($\Delta\sigma$) are in units of Å^2 sr^{-1}.

| Angle	15eV		20eV		25eV		30eV		40eV		50eV	
	σ	$\Delta\sigma$	σ	$\Delta\sigma$	σ	$\Delta\sigma$	σ	$\Delta\sigma$	σ	$\Delta\sigma$	σ	$\Delta\sigma$
20°							19.700	8.200	13.800	4.300	4.400	1.600
40°	5.900	2.200	2.050	0.570	3.000	1.100	1.940	0.560	1.430	0.420	1.270	0.380
60°	2.650	0.830	1.460	0.410	1.620	0.630	1.230	0.370	0.710	0.210	0.570	0.170
75°	1.470	0.430	0.860	0.240	0.840	0.330	0.650	0.200	0.430	0.130	0.320	0.098
90°	1.140	0.340	0.600	0.170	0.630	0.250	0.430	0.130	0.247	0.074	0.179	0.053
105°	1.230	0.410	0.700	0.200	0.730	0.300	0.510	0.160	0.303	0.098	0.169	0.052
120°	1.290	0.430	0.870	0.250	0.790	0.320	0.640	0.200	0.500	0.150	0.336	0.098
135°	1.920	0.610	1.020	0.300	1.090	0.430	0.930	0.280	0.750	0.230	0.650	0.200
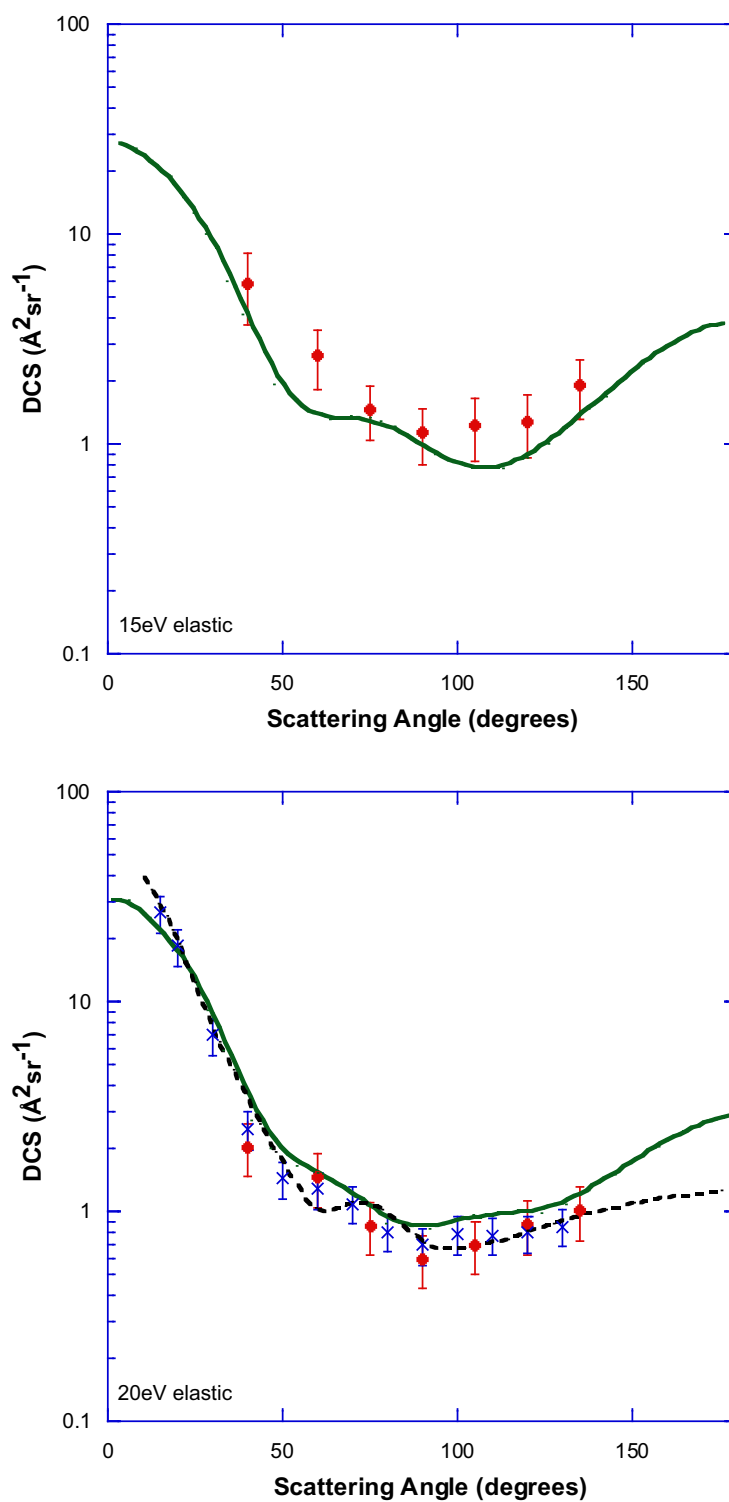
Figure 4.2.3: Absolute elastic DCS ($\mathring{A}^2 sr^{-1}$) for electron scattering from CF_3Br at incident energies of 15 and 20 eV. Present results obtained by the p-SSRDM ($\bullet$) normalisation are shown. Also shown are results from a previous effusive beam measurements [69] ($\times$), plus an SMCPP calculation result [70] (solid curve) and a CMS result [69] (dashed curve).
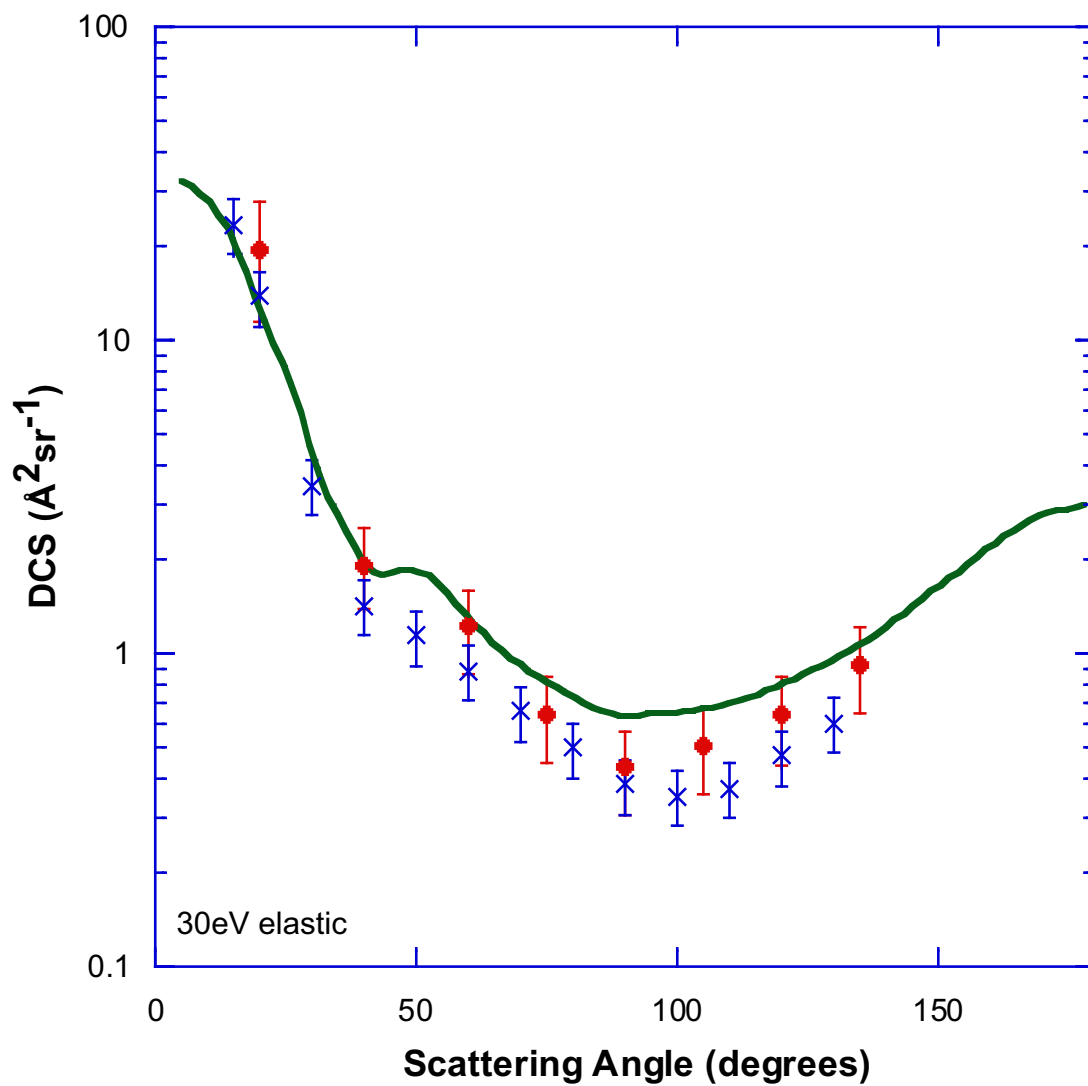
Figure 4.2.4: Absolute elastic DCS ($\text{Å}^2 sr^{-1}$) for electron scattering from CF_3Br at $30\,eV$ incident energy. Present results obtained by the p-SSRDM ($\bullet$) normalisation are shown. Also shown are results from a previous effusive beam measurements [69] ($\times$), plus an SMCPP calculation result [70] (solid curve).

Of these twelve fundamental vibrational modes, three were excluded from the adiabatic constant, as their energies are over 150 meV. These modes were the v_1 C-C stretch (232 meV), and the v_5 and v_9 asymmetric CF_2 stretch (166 meV). The adiabatic constant was thus evaluated as $\gamma=17/15$.

Supersonic beams of C_2F_4 have been used in previous experiments [71] as a mechanism for depositing thin polymer films of PTFE onto metal substrates. Therefore, the possibility of PTFE deposition on the stainless steel electron optics and chamber walls was considered. Had PTFE been deposited on the metal surfaces in the collision region, these surfaces would have potentially accumulated charge from the incident electron beam. Such a scenario would have adversely affected the performance of the monochromator and RFAs. However, both the incident beam current and the scattered electron count rates remained stable over the course of the measurements. This, coupled with the fact that there were no visible deposits when the collision chamber was opened after these measurements, suggests that PTFE deposition did not occur to any significant extent. In all likelihood, the molecular beam conditions in the collision region were not optimal for PTFE deposition. The optimal conditions for PTFE deposition include: stagnation pressures of several atmospheres; no use of a skimmer; placing the substrate in very close proximity to the nozzle (within a few millimetres); and using carrier gases to form the molecular beam. All of the above precautions serve to increase the C_2F_4 density at the substrate. That significant PTFE deposition was not observed in this research suggests that the molecular beam was not sufficiently dense for this to be an issue.

Absolute elastic DCSs for electron scattering from C_2F_4 were measured at incident energies between 15-50 eV (Figures 4.2.5 and 4.2.6), using the p-SSRDM normalisation with He employed as the reference species. For the C_2F_4 experiment, gas was introduced to the apparatus at stagnation pressures of 40 mbar (S_∞=5.4) for C_2F_4, and 45 mbar for He. As before, data was accumulated over four hours for both the C_2F_4 and He measurements, for each energy studied.

From a base pressure of 1.4×10^{-7} Torr, the pressure in the collision chamber when the gas was admitted rose to 3.3×10^{-7} Torr for C_2F_4 and 1.6×10^{-7} Torr for He. The ionisation cross section, $Q^{ion}=5.78\,\text{Å}^2$, for C_2F_4 was used for the p-SSRDM normalisation. The dimer formation parameter for this molecule was not explicitly evaluated, due to lack of suitable Lennard-Jones parameters. However, due to the present low stagnation pressures, clustering was not expected to be a significant issue here.

The total uncertainty in the present DCS measurements is approximately 35%, determined as the quadrature sum of statistical uncertainties ($<5\%$), normalisation uncertainties (25%) and the uncertainty on the He elastic DCS (7%).

The results of these measurements are given in Table 4.4, and plotted in Figures 4.2.5 and 4.2.6. The elastic SSRDM C_2F_4 DCSs were compared to a previous effusive beam result [72], plus two theoretical calculations. One of these calculations was made using the Kohn Variational Method [73], while the other used the SMC approach within a static exchange approximation [74]. The SSRDM cross sections are, to within their experimental uncertainties, in agreement with all of the previous data.

Due to the large number of vibrational modes available, the required stagnation pressure to allow the C_2F_4 beam to reach free-molecular flow at the skimmer was only 23 mbar. Unfortunately, in the present apparatus, the corresponding stagnation pressure of He (30 mbar) needed to match the speed ratio ($S_\infty=4.5$) resulted in an essentially undetectable pressure rise downstream of the skimmer. As a consequence, a stagnation pressure of 45 mbar was therefore used for He in this case, which was similar to the He stagnation pressure for the CF_3Br experiment. The stagnation pressure of C_2F_4 was therefore now set to 40 mbar to match the terminal speed ratio at the quitting surface, even though the quitting surface for C_2F_4 now occurred 7 cm upstream of the skimmer.
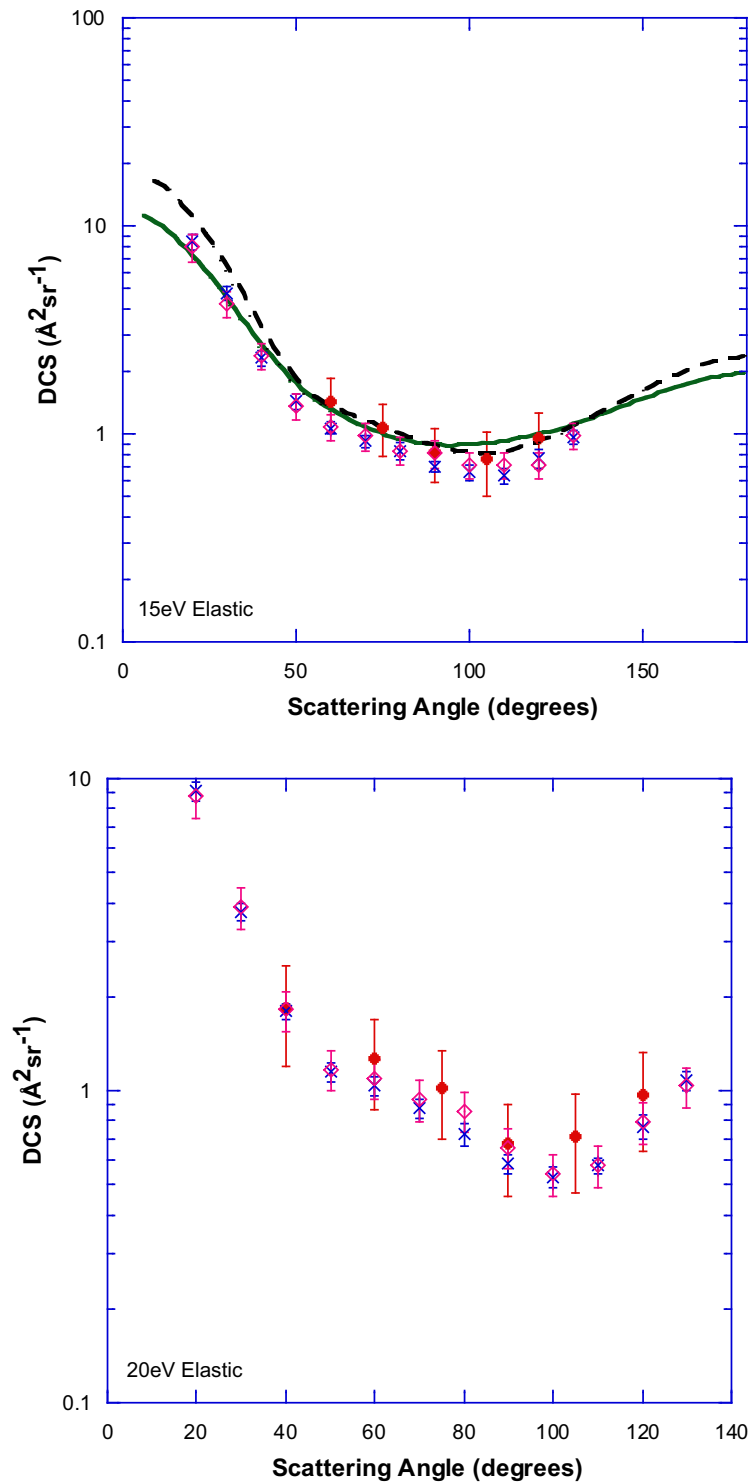
Figure 4.2.5: Absolute elastic DCS ($\mathring{A}^2 sr^{-1}$) for electron scattering from C_2F_4 at incident energies of 15 and 20 eV. Present results obtained by the p-SSRDM (•) normalisation are shown. Also shown are the ANU (×) and Sophia (◇) effusive beam measurement results [72], plus results from a Kohn variational calculation [73] (solid curve) and an SMC calculation [74] (dashed curve).
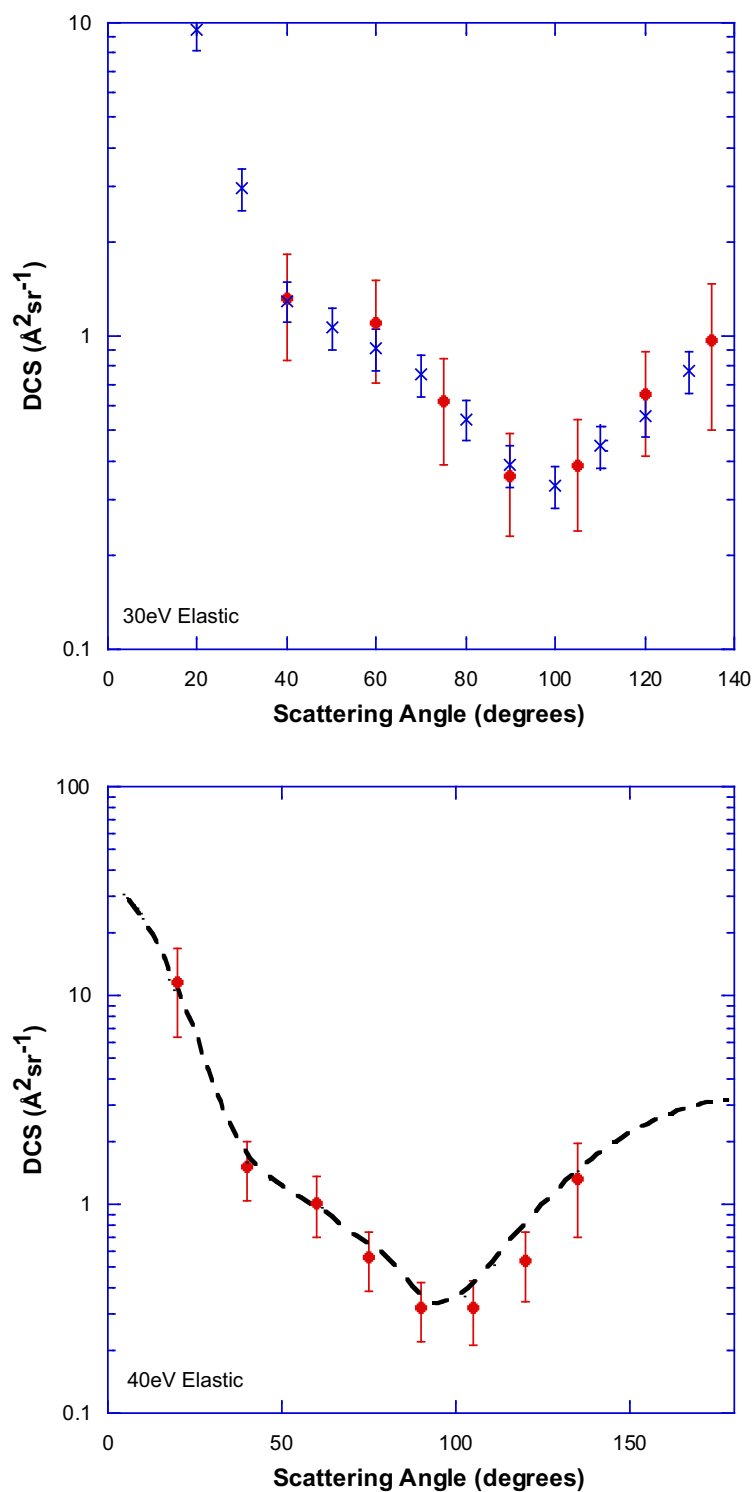
Figure 4.2.6: Absolute elastic DCS ($\mathring{A}^2 sr^{-1}$) for electron scattering from C_2F_4 at incident energies of 30 and 40 eV. Present results obtained by the p-SSRDM ($\bullet$) normalisation are shown. Also shown are the ANU ($\times$) and Sophia ($\diamond$) effusive beam measurement results [72], plus results from an SMC calculation [74] (dashed curve).

Table 4.4: Absolute elastic DCS for electron scattering form C_2F_4 at various energies determined by the p-SSRDM normalisation. The cross sections (σ) and their respective absolute uncertainties ($\Delta\sigma$) are in units of $\text{Å}^2 \, sr^{-1}$.

Angle	15eV		20eV		30eV		40eV		50eV	
	σ	$\Delta\sigma$	σ	$\Delta\sigma$	σ	$\Delta\sigma$	σ	$\Delta\sigma$	σ	$\Delta\sigma$
20°									3.800	1.300
40°			1.860	0.660	1.330	0.490	1.560	0.480	1.120	0.340
60°	1.440	0.420	1.280	0.410	1.110	0.400	1.030	0.330	0.580	0.170
75°	1.090	0.310	1.020	0.320	0.620	0.230	0.560	0.320	0.287	0.086
90°	0.830	0.240	0.680	0.220	0.360	0.150	0.320	0.100	0.183	0.055
105°	0.760	0.260	0.720	0.250	0.390	0.150	0.320	0.110	0.179	0.054
120°	0.970	0.290	0.980	0.340	0.660	0.240	0.540	0.200	0.460	0.140
135°					0.980	0.480	1.330	0.630	0.860	0.260

Since the stagnation pressure used here was in excess of that required for free molecular flow at the skimmer (equation 3.2.4), the scattering volumes of the C_2F_4 and He beams may not have been precisely matched. However, as the present C_2F_4 DCSs are in good agreement with the existing data [72], this would indicate that the scattering volumes were, at least approximately, matched. Possible explanations for the scattering volumes still being matched are that the description of the downstream molecular beam profile (equation 3.2.3) remains a fair approximation, even if free molecular flow at the skimmer is not strictly observed. Another explanation may be that the calculation of the quitting surface position (equation 3.2.4) tends to overestimate x_q as $\gamma{\rightarrow}1$. Alternatively, perhaps a quitting surface model is a little crude for the description of a low stagnation pressure supersonic expansion. The quitting surface model approximates the transition from collisional to molecular flow as a sudden change at a spherical surface. Since in reality this transition occurs over a region, perhaps for low pressure expansions this region is sufficiently large that the gas jet reaches a state of quasi-free molecular flow well upstream of the predicted quitting surface position. Thus, while in general the current DCS data sets of stable atoms and molecules are concluded to validate the SSRDM approach to cross section normalisation, caution is recommended when applying this method to expansions of polyatomics that contain more than six atoms.

4.2.4   900°C C_2F_4

Having validated the SSRDM approach for normalising supersonic beam DCSs, the pyrolysis tube was mounted in front of the nozzle so that effect of heating the target beam on the measured DCS could be studied. Because the pyrolysis nozzle needed to be set in excess of 1000°C to generate CF_2 radicals, these radicals would be formed with a significant population in their excited vibrational modes. Vibrational cooling of CF_2 by a supersonic expansion is only moderate, leaving the CF_2 products with vibrational temperatures of ≈1000°C unless extreme expansion conditions are applied. Such extreme expansion conditions include employing stagnation pressures of several atmospheres, nozzles diameters of

<0.1 mm and the use of carrier gases [24]. Such stagnation conditions are not feasible in the present apparatus, due to the restrictions of SSRDM normalisation and signal considerations. Therefore, the possibility of temperature related effects in a heated DCS, relative to the room temperature measurements, was investigated. This investigation was conducted by setting the pyrolysis nozzle at 900°C (just prior to the onset of C_2F_4 pyrolysis [24]) and re-measuring the DCS of C_2F_4. The results of this measurement were then compared to the room temperature data (Figure 4.2.7) to check for any differences.

The pyrolysis nozzle was installed, set to a temperature of 900°C and the 50 eV DCS for C_2F_4 was re-measured (Figure 4.2.7) using the p-SSRDM normalisation, with CF_4 employed now as the reference species. The stagnation pressure of both gases was set at 400 mbar, and the CF_4 elastic DCS results from a previous study [64] were used for the p-SSRDM normalisation. The SSRDM measurements of the CF_4 DCS were not used for this normalisation, as the data from the literature was determined to within tighter uncertainty limits.

In order match the speed ratios of the two beams, CF_4 was preferred as the reference species. A polyatomic reference was chosen because equation (3.2.10) does not describe the speed ratio's dependence on the stagnation temperature. Therefore, had He been chosen as the reference species, calculating the speed ratio of C_2F_4 to match with that for He would have been problematic. However, since equation (3.2.10) also indicates that the terminal speed ratios for all polyatomics are essentially similar, a polyatomic reference species was chosen. By using a polyatomic reference, the speed ratios of the two polyatomics could be assumed to be the same, provided the stagnation temperature and pressure matched.

Figure 4.2.7 clearly shows that the results from the heated measurement were completely consistent with the room temperature data. Since the room temperature measurement used a different reference species (He) and did not have the pyrolysis tube mounted in front of the nozzle, a number of conclusions were
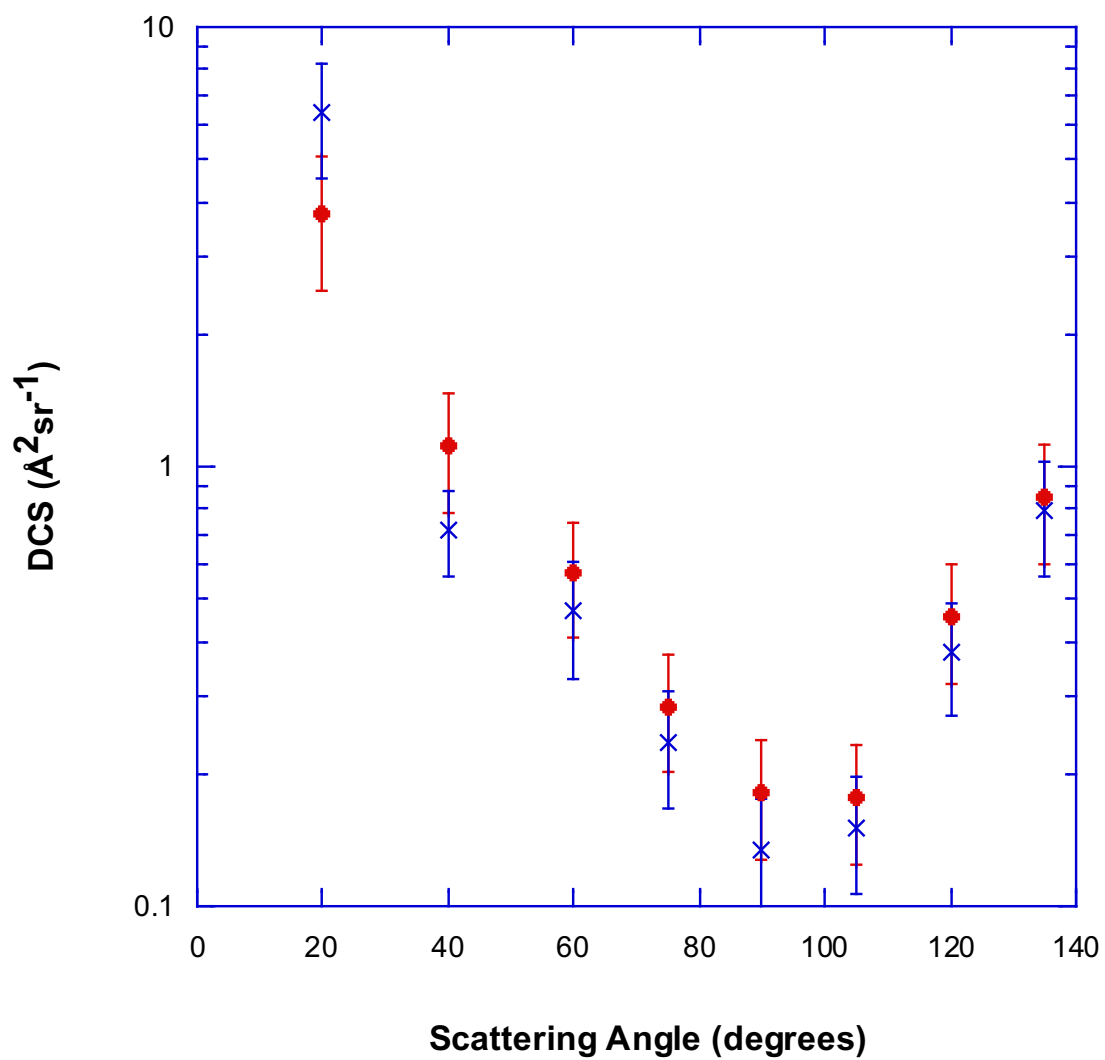
Figure 4.2.7: Absolute elastic DCS ($\mathring{A}^2 sr^{-1}$) for electron scattering from C_2F_4 at $50\,\mathrm{eV}$. Present results obtained by the p-SSRDM are shown for a room temperature expansion ($\bullet$) and a $900°C$ expansion ($\times$). The two data sets are clearly consistent to within their combined uncertainties.

drawn from this observation. Firstly, heating the source gas was concluded to not significantly effect the measured DCS, at least in the present energy range. Secondly, the assumption that supersonic expansions of heated polyatomic molecules were approximately equivalent under equivalent stagnation conditions was verified. Finally, the presence of the pyrolysis tube in front of the nozzle was concluded not to significantly affect the SSRDM description of the expanding beam dynamics, a result consistent with a previous study [35].

4.3 CF_2 Production

4.3.1 Decomposition Efficiency of C_2F_4

Having validated that the SSRDM accurately normalised the DCS of the target beam of interest, including when the beam temperature was initially above room temperature, attention now turned to producing a beam of CF_2 radicals. A molecular beam containing CF_2 radicals was formed by flowing C_2F_4 through the heated pyrolysis tube. Studies of the thermal decomposition of C_2F_4 by flash pyrolysis [24,33], as well as in shock tubes [75], have been previously reported in the literature. All of those studies concluded that CF_2 formation was the only C_2F_4 pyrolysis pathway of any consequence at temperatures below 2600°C.

To characterise the dissociation process, C_2F_4 was introduced into the system at a stagnation pressure of 400 mbar and the C_2F_4 intensity in the TOFMS was monitored as the nozzle temperature was increased from room temperature up to 1200°C. At each temperature, data in the TOFMS was accumulated over 200 laser shots. Background C_2F_4 intensity was also measured by accumulating a second TOF spectrum over 200 laser shots at each temperature, but this time triggering the YAG in between the gas pulses. The elastically scattered electron count rate, of 50 eV electrons in the 75° detector was recorded simultaneously with the TOF data to monitor the total molecular beam density. The scattered electron counts were accumulated over approximately 5 minutes.

The obtained results over the entire temperature range, ie. starting from room temperature, are shown in Figure 4.3.1 as a function of the electrical power through the pyrolysis tube. The results in Figure 4.3.2 show the same data as function of the pyrolysis tube temperature, for those data points where the temperature was in excess of 700°C, below which the pyrolysis tube did not radiate and hence the pyrometer could not measure the temperature.

The TOFMS intensity and scattered electron counts scaled proportionally with the nozzle power until the nozzle temperature reached approximately 40 W (Figure 4.3.1), at which point the nozzle temperature was 900°C. As the pyrolysis temperature was then further raised, the intensity of C_2F_4 in the TOFMS decreased more rapidly than did the scattered electron intensity. The onset of pyrolysis was thus concluded to be at approximately 900°C, a result consistent with those from previous studies [24, 33].

The dissociation data is also shown plotted as a function of the nozzle temperature (Figure 4.3.2) over the temperature range which could be monitored by the pyrometer. At approximately 1200°C, the C_2F_4 intensity decreased to below the detection limit of the TOFMS, while the scattered electron counts remained at approximately 45% of the pre-pyrolysis intensity. Therefore, C_2F_4 was concluded to decompose with approximately unit efficiency at 1200°C.

With a first ionisation energy at 11.45 eV [76], CF_2 radicals cannot be ionised by a single 118 nm photon (10.48 eV). The TOFMS was therefore unable to directly detect CF_2 radicals. A previous study of C_2F_4 [24] pyrolysis found that formation of CF radicals, due to pyrolysis of the CF_2 products, was the second pyrolytic pathway for C_2F_4 decomposition. With a first ionisation energy of 9.11 eV [77], CF radicals could be detected in the TOFMS, if they were present in the molecular beam. However, with the nozzle temperature set to 1200°C, no evidence for CF radical production was observed in the TOFMS. Thus, CF production was concluded not to be occurring at a pyrolysis temperature of 1200°C. Similarly no other fluorocarbon radicals with ionisation energies below 10.48 eV, such as
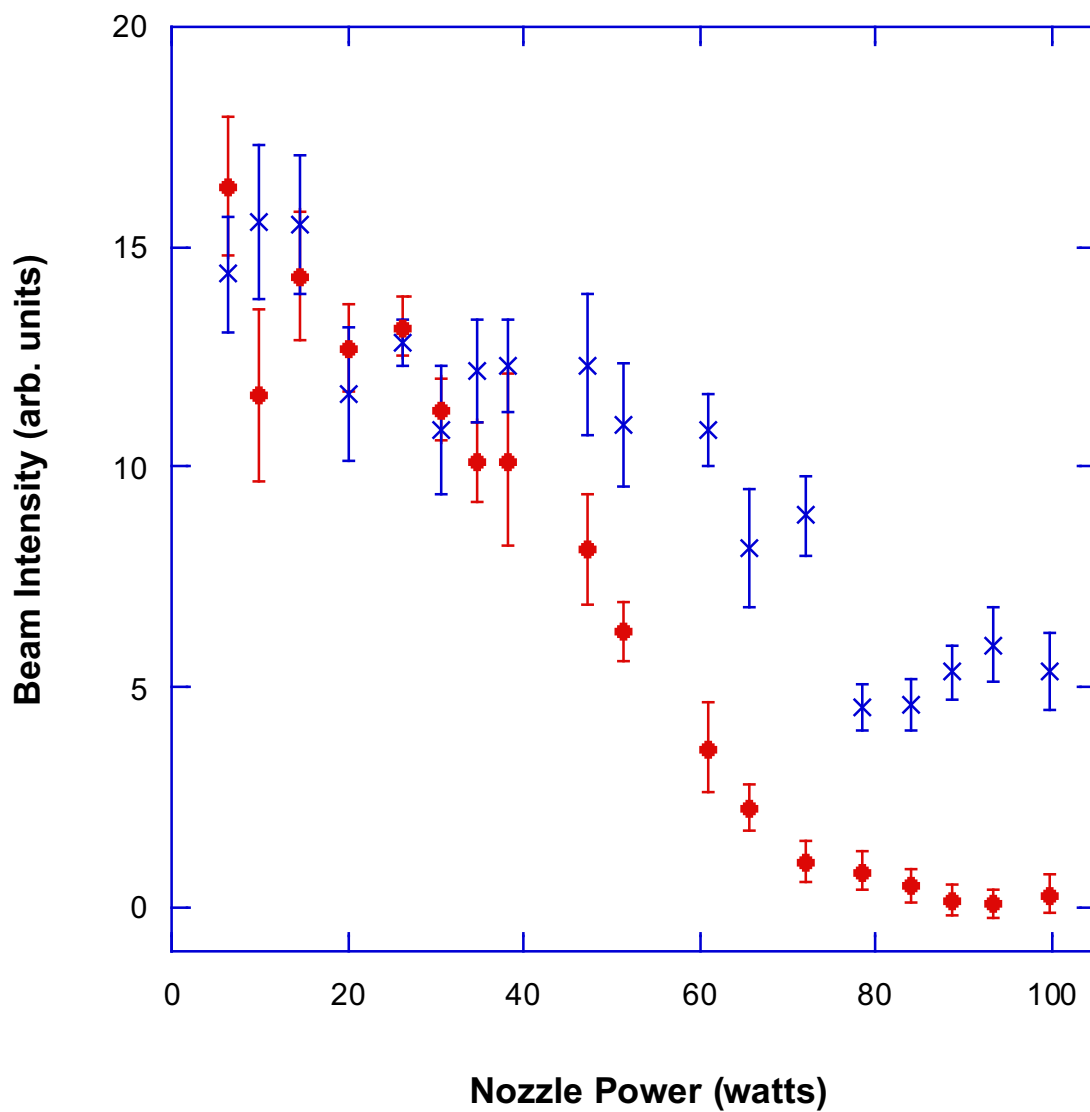
Figure 4.3.1: C_2F_4 intensity ($\bullet$) measured in the TOFMS and elastically scattered electron counts ($\times$), as measured in the 75° detector, plotted as a function of electrical power through the pyrolysis tube. The error bars represent the statistical variations in the C_2F_4 intensity and the scattered electron counts.
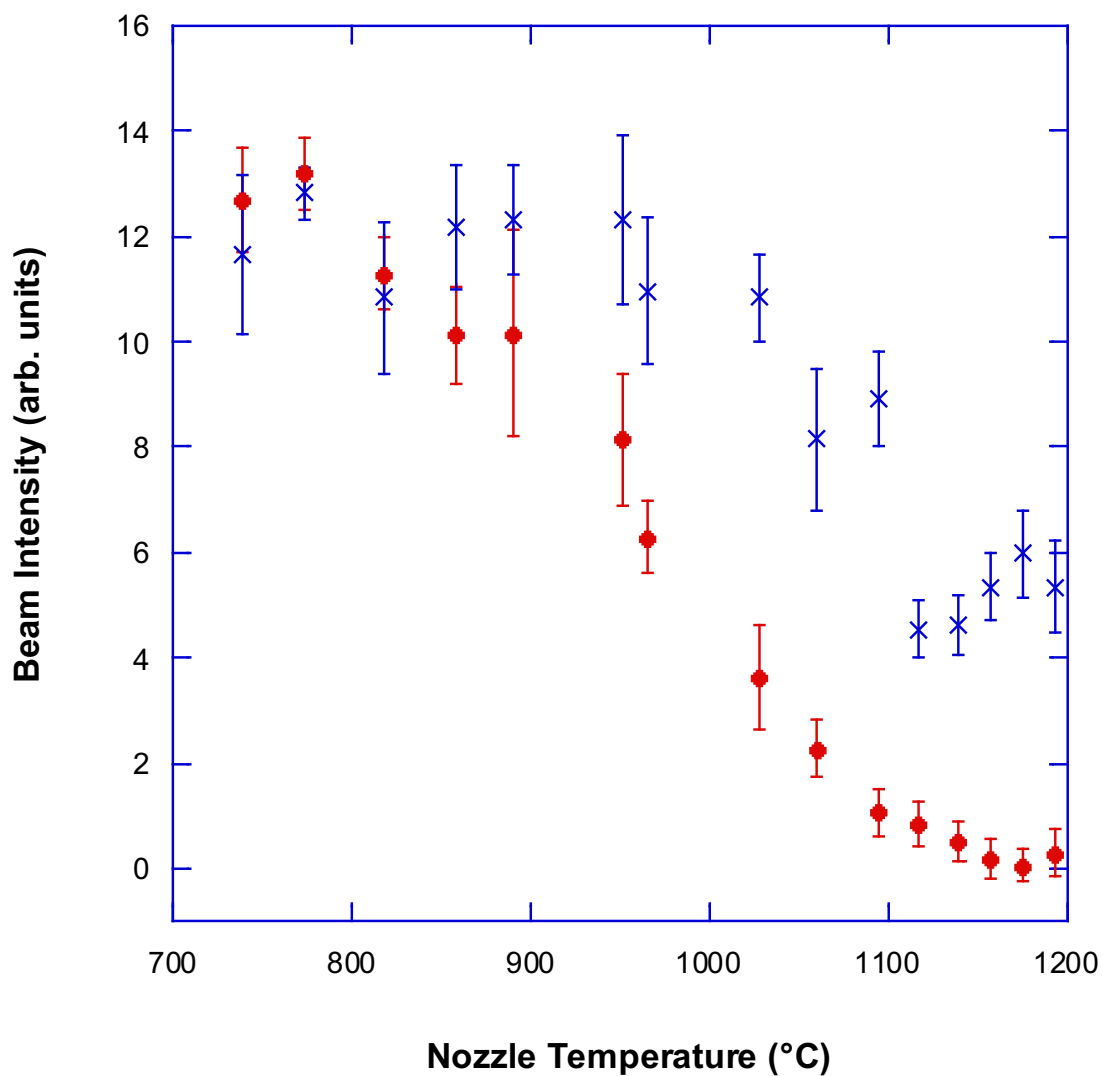
Figure 4.3.2: C_2F_4 intensity (•) measured in the TOFMS and elastically scattered electron counts (×), as measured in the 75° detector, plotted as a function of pyrolysis tube temperature. The error bars represent the statistical variations in the C_2F_4 intensity and the scattered electron counts.

CF$_3$ (IE=8.76 eV [78]) or C$_2$F$_3$ (IE=10.20 eV [79]), were detected in the TOFMS. Based on these observations of unit decomposition efficiency of C$_2$F$_4$ at 1200°C and no production of CF or any other radicals, the molecular beam was concluded to be composed predominantly of CF$_2$ radicals.

4.3.2 Stagnation Pressure Mismatch

Having established that the pyrolysed molecular beam was comprised almost entirely of CF$_2$ radicals, the DCSs of CF$_2$ were measured using the p-SSRDM normalisation, with CF$_4$ as the reference gas. CF$_4$ was chosen as the reference species for two reasons. One reason, just noted in the previous section, was that a polyatomic reference was required to measure the cross section of a heated polyatomic target. The second reason for choosing CF$_4$ as the reference species was that CF$_4$ does not pyrolyse at 1200°C.

Before making extensive measurements for the elastic DCS of CF$_2$, the influence of stagnation pressure on the measured radical DCS was investigated. The speed ratio of the molecular beams is dependent on the stagnation pressure, and the speed ratios of the two molecular beams must match. Because C$_2$F$_4$ pyrolyses into two CF$_2$ radicals there was the possibility that the effective CF$_2$ stagnation pressure in the pyrolysis tube was actually twice as high as that measured upstream by the Baratron. Since CF$_4$ does not pyrolyse at 1200°, the effective stagnation pressures of the two beams may have been mismatched. Since a mismatch in the stagnation pressures would cause a mismatch in the speed ratios, this possibility was investigated.

Two measurements of the elastic DCS for electron scattering from CF$_2$ were hence made using p-SSRDM normalistation, at 50 eV incident energy, with CF$_4$ employed as the reference species. The temperature of the nozzle was set at 1200°C to ensure that the C$_2$F$_4$ was completely pyrolysed, but that the temperature was still sufficiently low so as not to allow any secondary pyrolytic pathways. The ionisation cross section for the p-SSRDM normalisation were

taken as Q^{ion}=1.77 Å^2 for CF$_2$ [28]. The stagnation pressure of C$_2$F$_4$ was set at 400 mbar. For CF$_4$, however, two measurements were made, one with the stagnation pressure set to 400 mbar, and the other at 800 mbar. If the stagnation pressure of CF$_2$ was really twice as high as the Baratron recorded, then the 800 mbar experiment should account for the asymmetry. Both sets of measurements were accumulated over 2 hours.

The two resulting DCS measurements are consistent with each other to within their respective uncertainties (Figure 4.3.3). This result is also consistent with the previous results for the C$_2$F$_4$ DCS, where the collision volumes of the target and reference beams were thought to be possibly mismatched, yet accurate DCSs were still obtained. Therefore the stagnation pressure was concluded to not significantly effect the measured DCS in this incident energy range, provided the centreline density of each beam was properly accounted for by the pressure rise.

4.4 Differential Cross Sections for CF$_2$ radicals

With the pyrolysed molecular beam determined to consist almost exclusively of CF$_2$ radicals, and no observable effects found in the DCS measurements caused by the elevated temperature of the targets or the pyrolysis, the elastic DCSs for the CF$_2$ radical were measured (Figures 4.4.1-4.4.4), between 25-50 eV incident electron energy, using the p-SSRDM normalisation and employing CF$_4$ as the reference species. As noted previously, CF$_2$ was formed by pyrolysis of C$_2$F$_4$, with the C$_2$F$_4$ and CF$_4$ stagnation pressures both set at 400 mbar. The pyrolysis nozzle was set to 1200°C to ensure full conversion of C$_2$F$_4$ into CF$_2$. Data was accumulated over four hours for both the CF$_2$ and CF$_4$ beams, with the measured DCS data being given in Table 4.5.

The total uncertainty in these DCS measurements is between 35-40%, determined as the quadrature sum of statistical uncertainties ($<$5%), normalisation uncertainties (25%) and the uncertainty of the CF$_4$ elastic DCS (20%).
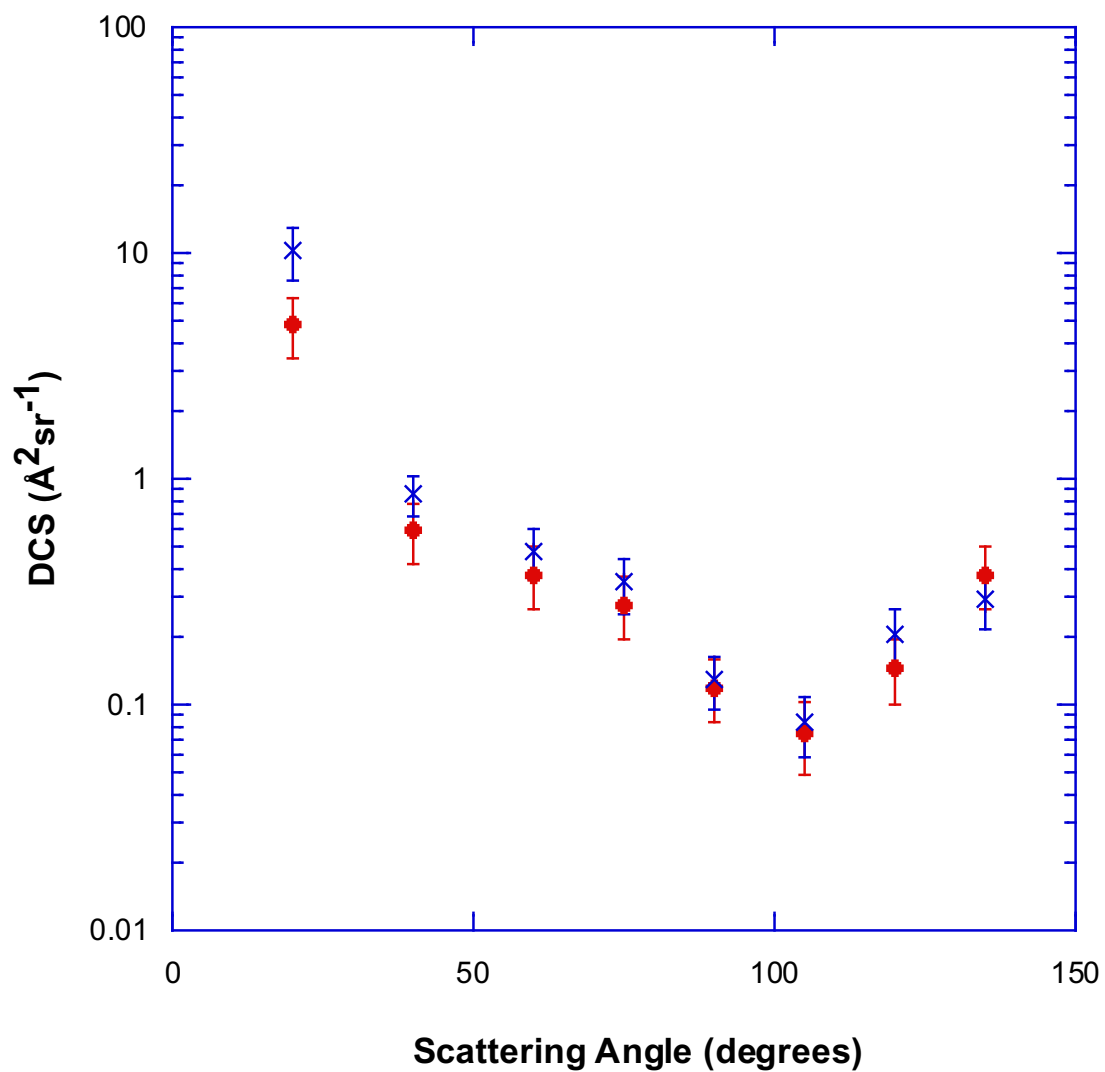
Figure 4.3.3: Absolute elastic DCS ($\text{Å}^2 sr^{-1}$) for electron scattering from CF_2 at $50\,\text{eV}$. These results were obtained by the p-SSRDM normalisation using a CF_4 reference. The stagnation pressure ratios of CF_2:CF_4 are 1:1 (•) and 1:2 (×). The two data sets are clearly consistent to within their combined uncertainties.

Integral cross sections, ICS, (Figure 4.4.5) and momentum transfer cross sections, MTCS, (Figure 4.4.6) were subsequently derived from the measured DCS data, with the angular range of the measured DCS extrapolated to 0° and 180° using a molecular phase shift analysis technique [80], prior to the usual integration being performed. Namely the ICS and MTCS, at a given energy, were determined using the following equations:

$$ICS = 2\pi \int_0^\pi sin\,(\theta)\,DCS(E_0, \theta)d\theta, \qquad (4.4.1)$$

$$MTCS = 2\pi \int_0^\pi (1 - cos\,(\theta))\,sin\,(\theta)\,DCS(E_0, \theta)d\theta, \qquad (4.4.2)$$

where E_0 is the incident electron energy, and θ is the electron scattering angle.

The derived ICS and MTCS values are also included in Table 4.5. The uncertainties on the ICSs and MTCSs are estimated at approximately 45%. These ICS uncertainties were estimated by recording the variation in the derived ICS over a reasonable range of extrapolated DCS values. This variation was then combined with the ~35% uncertainty in the DCS to arrive at a total uncertainty of ≈45% in the integrated values.

4.4.1 Comparison With Theory

The current DCS and ICS measurements are compared to a series of results calculated using various theoretical methods including: the ISVM [32]; the SEP approximation [13] and the R-Matrix approach [31]. Before discussing the comparison of the experimental and theoretical data, a brief overview of the various theories is now given.

The R-Matrix method considers the scattering problem divided into two regions, an inner and outer centred on the target molecule. The inner region is typically represented as a sphere of radius $10a_0$, where a_0 is the Bohr radius. Inside this inner region, the electron exchange and electron-electron correlation effects are modelled using various quantum chemistry methods. In the outer region, long
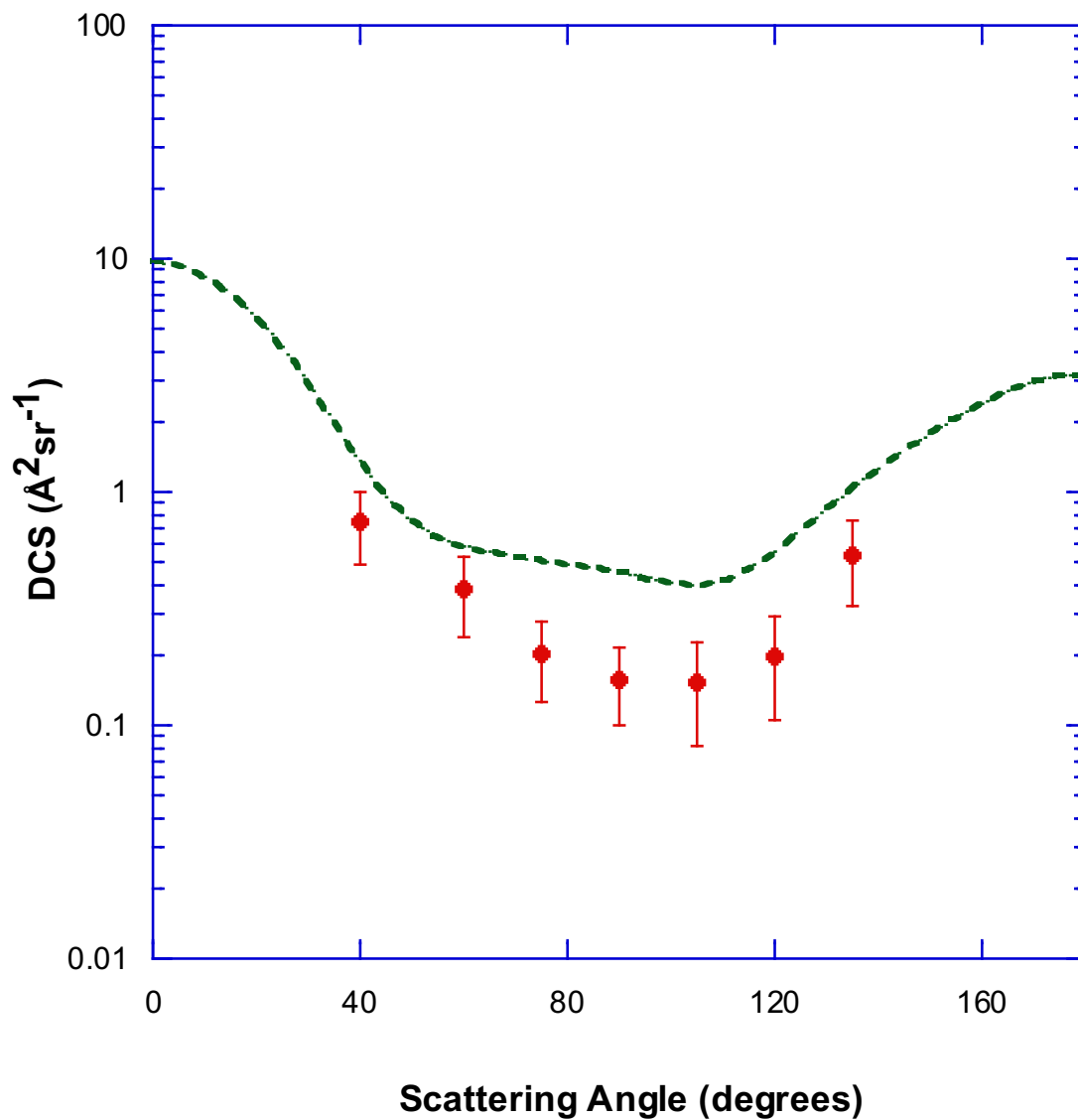
Figure 4.4.1: 25 eV absolute elastic DCSs ($\text{Å}^2 sr^{-1}$) for electron scattering from CF_2. Present results (●), obtained by the p-SSRDM normalisation, are shown. Also shown is the result of an SEP calculation [13] (dashed curve).
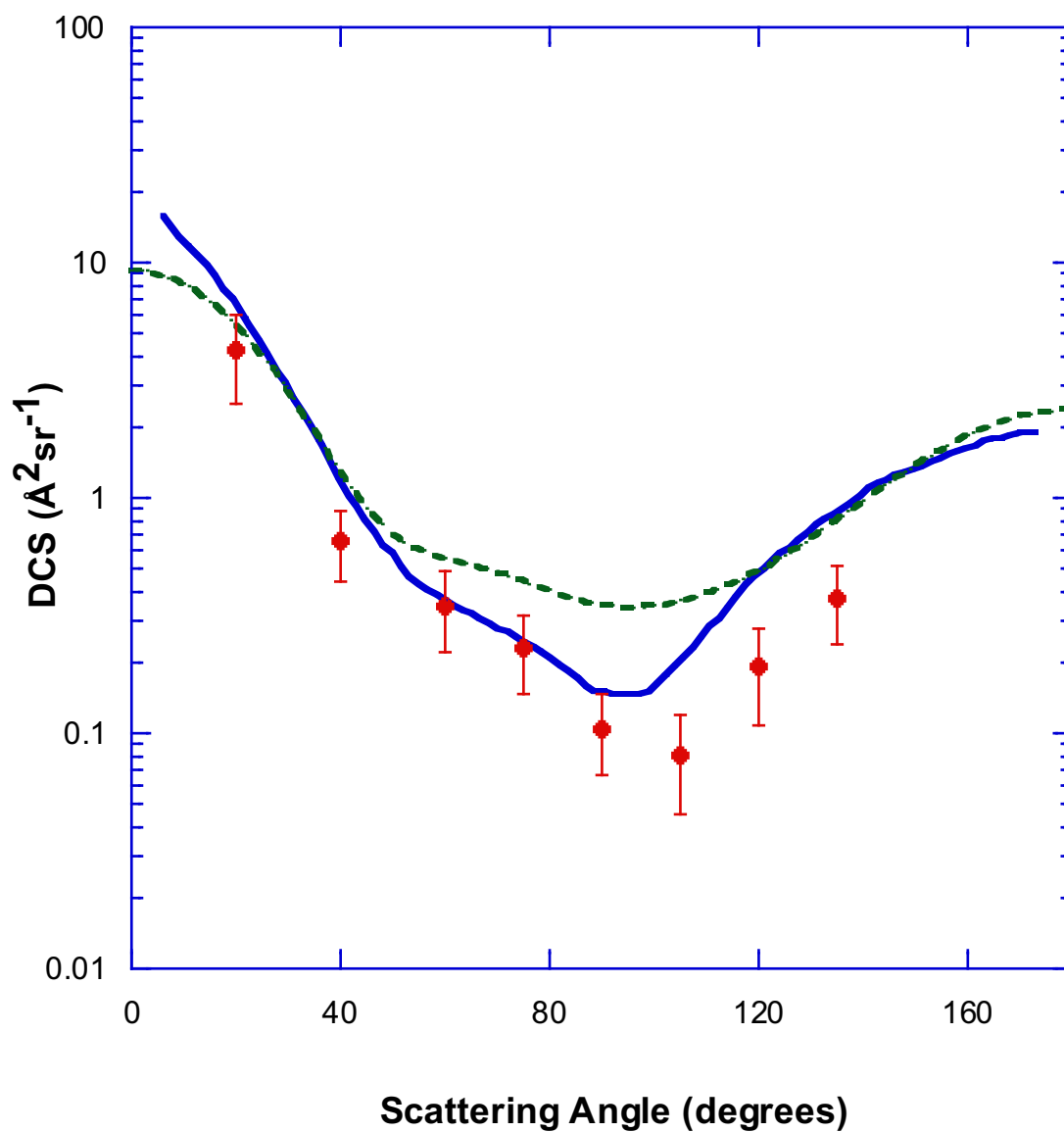
Figure 4.4.2: 30 eV absolute elastic DCSs ($\text{Å}^2 sr^{-1}$) for electron scattering from CF_2. Present results (●), obtained by the p-SSRDM normalisation, are shown. Also shown are the results from an ISVM calculation [32] (solid curve) and an SEP calculation [13] (dashed curve).
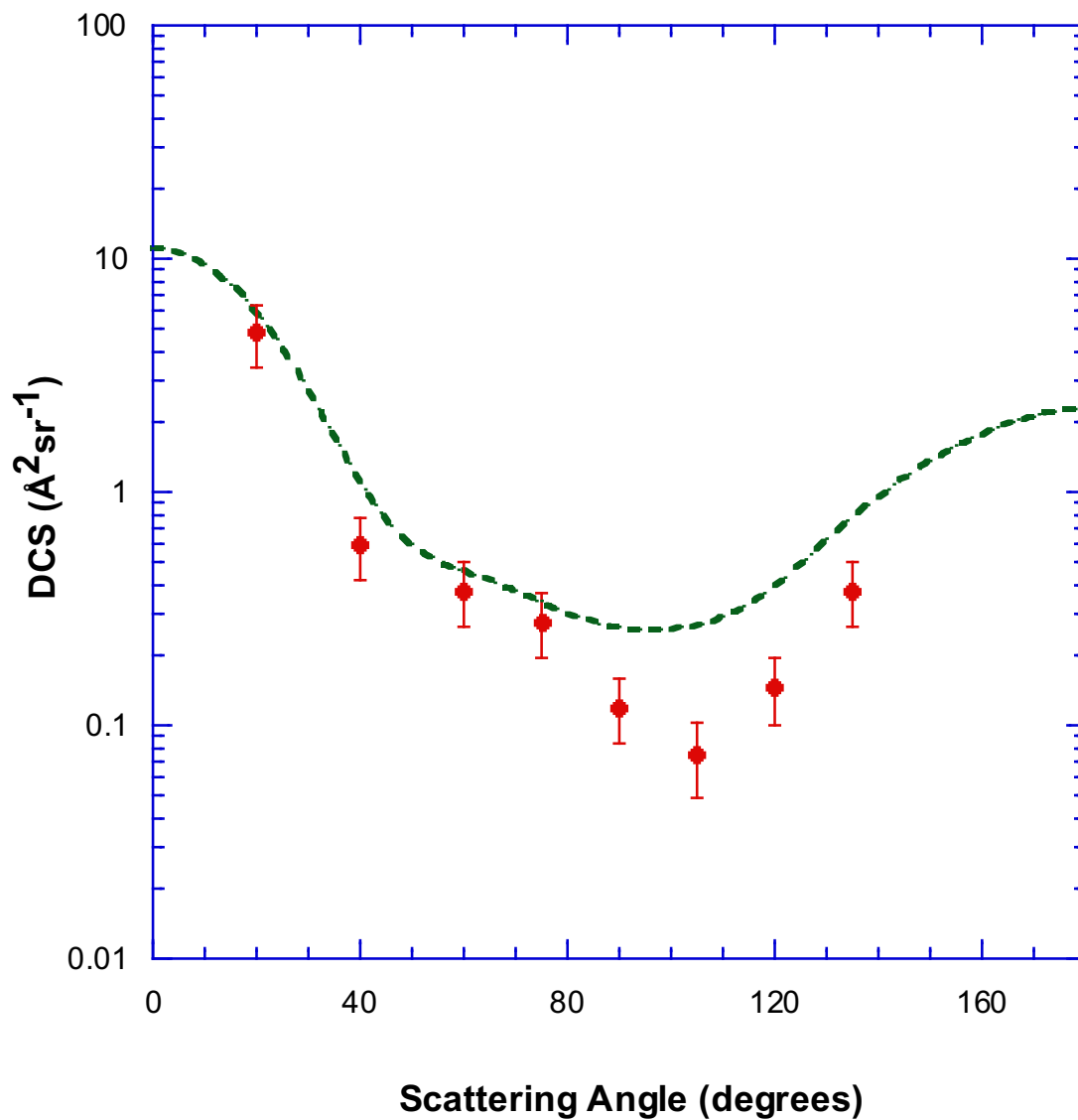
Figure 4.4.3: $40\,\mathrm{eV}$ absolute elastic DCSs ($\mathring{A}^2 sr^{-1}$) for electron scattering from CF_2. Present results ($\bullet$), obtained by the p-SSRDM normalisation, are shown. Also shown is the result of an SEP calculation [13] (dashed curve).
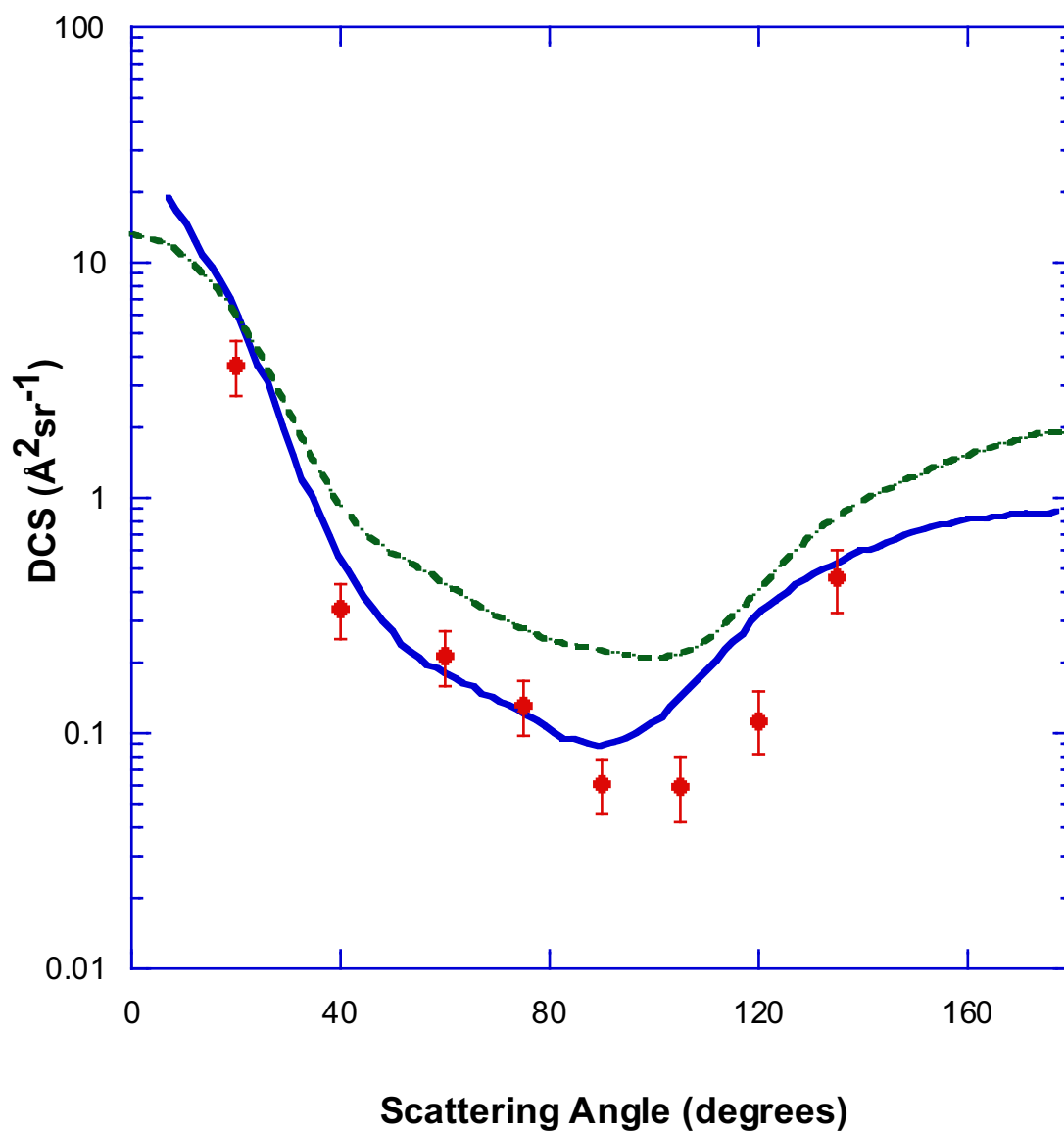
Figure 4.4.4: 50 eV absolute elastic DCSs ($\mathring{A}^2 sr^{-1}$) for electron scattering from CF_2. Present results ($\bullet$), obtained by the p-SSRDM normalisation, are shown. Also shown are results from an ISVM calculation [32] (solid curve) and an SEP calculation [13] (dashed curve).
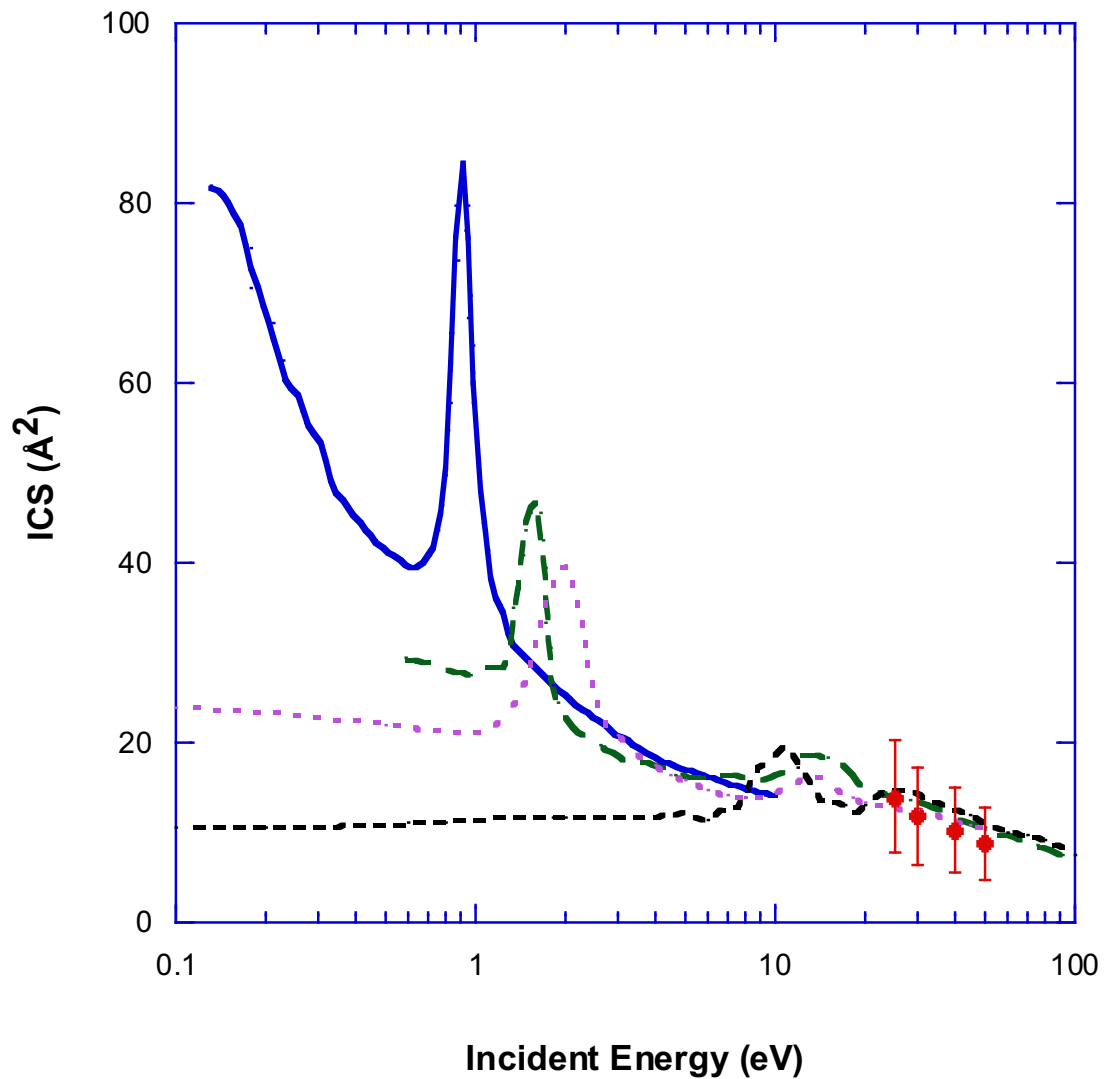
Figure 4.4.5: Absolute elastic ICSs (Å^2) for electron scattering from CF_2 at incident energies between 1-100 eV. Present results (•), obtained by the p-SSRDM normalisation, are shown. Also shown are the results from an R-Matrix calculation (solid curve), an ISVM calculations(long dashed curve), an SEP calculation (short dashed curve), and an SE calculation (dotted curve) [13].

Figure 4.4.6: Absolute MTCSs ($\mathring{A}^2$) for electron scattering from CF_2 at incident energies between 1-100 eV. Present results (●), obtained by the p-SSRDM normalisation, are shown. Also shown are the results from an R-Matrix calculation [31] (solid curve), an ISVM calculations [32] (long dashed curve), an SEP calcuation (short dashed curve), and an SE calculation (dotted curve) [13].
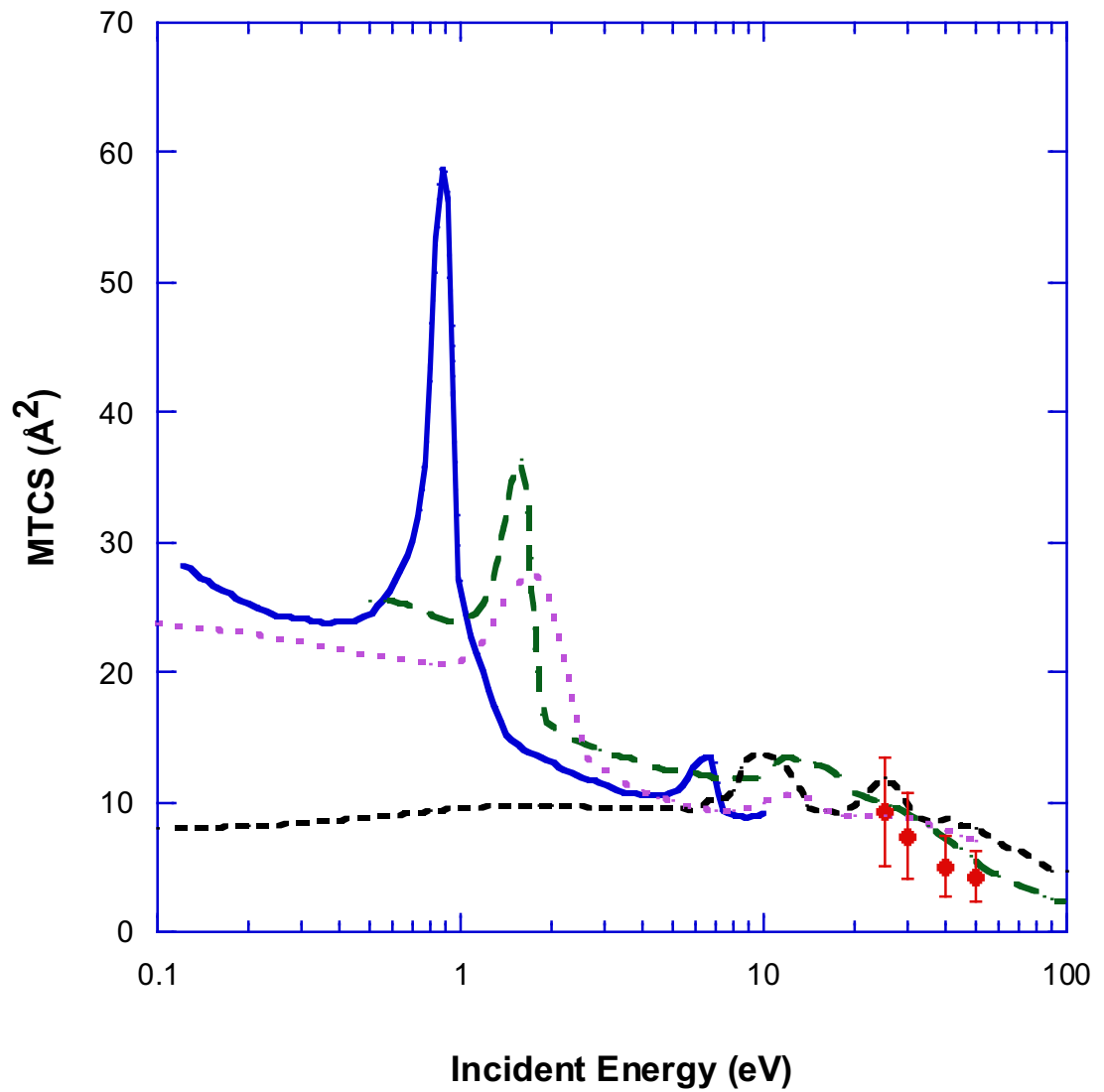
Table 4.5: Absolute elastic DCSs for electron scattering from CF_2 at various energies determined by the p-SSRDM normalisation. The cross sections (σ) and their respective absolute uncertainties ($\Delta\sigma$) are in units of $\text{Å}^2\,sr^{-1}$. Also included in the table are the respective ICSs and MTCSs, in units of Å^2.

Angle	25eV		30eV		40eV		50eV	
	σ	$\Delta\sigma$	σ	$\Delta\sigma$	σ	$\Delta\sigma$	σ	$\Delta\sigma$
20°			4.200	1.700	4.900	1.500	3.700	1.500
40°	1.210	0.420	0.660	0.220	0.600	0.180	0.338	0.088
60°	0.630	0.240	0.350	0.130	0.380	0.110	0.215	0.056
75°	0.330	0.130	0.232	0.086	0.280	0.084	0.131	0.035
90°	0.258	0.095	0.107	.040	0.120	0.036	0.061	0.016
105°	0.250	0.120	0.082	0.037	0.075	0.026	0.060	0.018
120°	0.320	0.150	0.195	0.086	0.147	0.047	0.115	0.034
135°	0.860	0.350	0.380	0.140	0.380	0.120	0.460	0.140
ICS	14.00	6.30	11.80	5.30	10.30	5.10	8.30	3.70
MTCS	9.30	4.20	7.32	3.30	4.60	2.30	4.30	1.90

range effects are considered the dominant factors in the interaction between the electron and target. The inner region scattering wavefunction, Ψ, for an arbitrary N electron molecules is given as:

$$\Psi_k^{N+1} = A \sum_I \Psi_I^N (x_1, ..., x_N) \sum_j \zeta_j (x_{N+1}) a_{Ijk} + \sum_m \chi_m (x_1, ..., x_N, x_{N+1}) b_{mk}.$$

$$(4.4.3)$$

In the above equation, A is the anti-symmetrisation operator, x_n is the spatial and spin co-ordinate of the nth electron, ζ_j is a continuum orbital spin coupled with the scattering electron, a_{Ijk} and b_{mk} are variational coefficients, and the χ_m represent different configurations as electrons are allocated into the target molecular orbitals [31]. For the CF_2 calculation the target was represented, in its equilibrium geometry, using a 6311-G* Gaussian basis set, implemented using Complete Active Space Interaction Configuration wavefunctions.

Both the ISVM and SEP calculations are implementations of the Schwinger Multichannel Method, whereby the target Hamiltonian is approximated as the sum of the free Hamiltonian, H_0, and the kinetic energy operator, T_{N+1}, of the incident particle. Under this assumption the Lippmann-Schwinger equation [11] is solved to yield the differential cross sections.

The most significant difference between the two approaches is the description of the scattering potential employed. The SEP calculation includes static, exchange and polarisation contributions to the scattering potential, all modelled using a Hartree-Fock approximation. The ISVM also includes the previously mentioned contributions, calculated from Hartree-Fock self-consistent field wavefunctions. Both calculations employ a 6113-G Gaussian basis set. The ISVM, however, also includes a complex absorption contribution to the scattering potential, described as a quasi-free scattering model [81]. Finally, correlation-polarisation contributions are included using a parameter-free model for polarisation of molecules [82].

The current DCS measurements are compared to corresponding ISVM calculation results [32] and SEP calculation results [13]. There is generally good agreement between the experimental cross sections and both of the theoretical data sets, particularly at scattering angles <60°, although the current measurements somewhat favour the ISVM approach over the SEP calculation. Both calculations, however, exceed the measurements by more than the experimental uncertainties at backward scattering angles, with the SEP calculation again exhibiting a larger discrepancy to the measurements than that for the ISVM.

Since CF_2 is a moderately polar molecule [25], long-range dipole interactions are expected to dominate the low- to intermediate-energy DCS. Therefore, the description of both the permanent dipole moment and the induced polarisation used in the theoretical treatments are important considerations. The SEP calculation neglects the permanent dipole moment of CF_2 [13], while the ISVM uses a calculated value of $0.246\,D$ [32], which is approximately half of the experimental value. The magnitude of the cross sections in the forward scattering region are expected to increase approximately as square of the dipole moment [30]. As is consistent with this prediction, at angles <40° (Figures 4.4.1-4.4.4) the present results increase more rapidly than the SEP DCS at all energies studied. This behaviour is also found for the ISVM cross sections. Thus, the lack of inclusion of a dipole correction in the SEP calculation may at least partially explain why the ISVM treatment is in better accord with the current measurements.

As well as different descriptions of the dipole interactions, the degree of sophistication in coupling to the open inelastic channels varies. The ISVM results describe such coupling by an absorption potential [32]. The SEP also includes such coupling, however, all inelastic channels are treated as closed in that description [13]. This may also in part explain why the ISVM results appears to be in better accord with the present measurements than the corresponding SEP results.

The dipole polarisability of CF_2 is not a well known quantity. Calculations of its value, by different theories employing different basis sets, range from between

$6a_0^3$ to $17a_0^3$ [26] with no experimental value being available. As mentioned in the review of the literature (Section 1.2), a previous study of the TICS of CF_2 [28] found that in order to replicate corresponding experimental results, the long range dipole interactions had to be shielded. The authors of that study concluded, as noted earlier, that the strongly electronegative C-F bond reduced the long range dipole polarisation interaction potential of CF_2 from the value calculated using a Born approach. Since the permanent dipole moment of CF_2 is well understood, the evidence is that the current theoretical descriptions for the dipole polarisability may be less than adequate in the case of CF_2. Thus, a poor description of the induced polarisation in CF_2 may in part explain the consistent differences between the measured and calculated DCS, such as at the backward scattering angles.

The derived ICSs and MTCSs are also compared to various theoretical cross sections, including results from an R-Matrix calculation [31], ISVM results [32] and results from two Schwinger Multichannel calculations employing a static exchange approximation [13]. The first of these Schwinger calculations includes the polarization of the target (SEP), while the second neglects polarization effects (SE).

The present measured ICSs are consistent with the ISVM, SEP and SE results, while the R-Matrix calculation does not extend to sufficiently high enough energies to be directly comparable with the present measurements. The measured MTCSs are also, to within their experimental uncertainties, in agreement with the ISVM values, while the SEP and SE results exceed the magnitude of the current data at 40-50 eV incident electron energies.

The most notable feature of the calculated ICSs and MTCSs is the presence of a strong shape resonance, of $^2B_1$ symmetry, centred at around 1-2 eV, resulting from the incident electron temporarily occupying the $3b_1$ orbital of CF_2 [31]. While all four calculations predict this resonance, they vary significantly as to the value of its peak energy. The R-Matrix calculation places the resonance at 0.95 eV, the ISVM at 1.5 eV, the SEP at 10 meV (and thus below the energy limit

of Figure 4.4.5) and the SE at $2\,\text{eV}$. The magnitude of this resonance also varies between the different calculations, the R-Matrix calculation gives an amplitude (in the ICS) of $82\,\text{Å}^2$, the results from the ISVM approach say $49\,\text{Å}^2$ and the SE result finds $40\,\text{Å}^2$. A second, smaller, shape resonance of $^2B_2$ symmetry is also predicted at $\approx 15\,\text{eV}$ by each calculation, except for the R-Matrix which does not extend to this energy.

Excluding the resonance regions, at incident energies $>3\,\text{eV}$ and below $0.8\,\text{eV}$ the agreement between all of the calculations is quite good. The exception to this are the results of the SEP calculation, which are significantly lower than the other three. Above $10\,\text{eV}$ the agreement between all four calculations is excellent. The change in the ICS by adding polarisation into the SE calculation is quite marked below $10\,\text{eV}$. In principle the SEP approach is a more sophisticated, and hence presumably more accurate, calculation than the SE, which is the least computationally taxing calculation of the four. It is therefore interesting that the SE calculation appears in better accord with the more sophisticated R-Matrix and ISVM calculations than is the SEP.

Evidence has already been provided that suggests the polarisability of CF_2 is not well described by theory, with different descriptions yielding rather different results. All of the presented calculations employ a $(10s5p/4s3p)$ basis set, but the implementation methods used vary. The R-Matrix calculation employs a Complete Active Space Configuration Interaction description, the ISVM calculation uses a Hartree-Fock Self Consistent Field method while the SEP and SE approaches employ a second order Möller-Plesset Perturbation method. Since the description of the polarisation increases in importance as the incident electrons energy reduces, the differences between the calculated ICSs at the low energies are therefore possibly a result of their different descriptions of the polarisation.

Unfortunately the present measurements do not extend to sufficiently low energy to offer any insight into the discrepancies between the various theories in the

resonance regions. Clearly there is a need for an experimental investigation for the elastic ICS of CF_2 at sub-10 eV energies. While more investigation beyond that presented here is still necessary, the current result that the intermediate-energy ICSs of CF_2 are well described by a computationally cheap SE calculation is a significant finding.